STRATIGRAPHY AND DEPOSITIONAL CONTROLS ON SOURCE ROCK FORMATION WITHIN THE UPPER CRETACEOUS (LOWER CEMOMANIAN) MANESS SHALE, CENTRAL TEXAS

A Thesis

by

ANN MARIE HUDSON

Submitted to the Office of Graduate and Professional Studies of
Texas A&M University
in partial fulfillment of the requirements for the degree of

MASTER OF SCIENCE

Chair of Committee,	Michael M. Tice
Committee Members,	Bruce Herbert
	Juan Carlos Laya
Head of Department,	John R. Giardino

December 2014

Major Subject: Geology

ABSTRACT

With the success of the prolific Eagle Ford Shale play in South Texas, there is increasing interest in the resource potential of its equivalent source rock on the northeast side of the San Marcos Arch. The "Eagle Ford Shale" northeast of the San Marcos arch is composed of the transgressive lower Cenomanian Maness Shale, which unconformably overlies the Buda Limestone, and the regressive upper Cenomanian Pepper Shale of the Woodbine Group which unconformably underlies the Austin Chalk. This succession has sourced multiple reservoirs within the western portion of the East Texas Basin and is now being evaluated as a potential self-sourced reservoir. In this study we will attempt to determine the depositional controls on the formation of organic-rich source rock within the Maness Shale and divide the interval into chemostratigraphic packages based on whole rock elemental data. The main goals are 1) to build a depositional model within a sequence stratigraphic framework that can be used as a predictive tool to locate the richest source rocks within the basin, and 2) to determine the distribution of source rock facies vertically and laterally across the basin.

The Maness Shale is a mixed carbonate and siliciclastic mudrock which contains overall high TOC and was deposited in an anoxic, low-energy environment. Maximum TOC and carbonate content are found within a condensed section located in the upper portion of the Maness Shale in association with a maximum flooding surface. Paleo-redox elements (Cu, Ni, V, Mo, and U) indicate that maximum levels of anoxia were reached within the condensed section. Carbonate content is thought to be biogenic in

origin and is a result of increased productivity within the basin. Increases in productivity also lead to a high amount of organic material being deposited and preserved.

ACKNOWLEDGEMENTS

I would like to thank Apache Corporation for graciously allowing me to pursue this research while under their employment as a full time Geologist and for providing me with all the data included in the study. My sincere thanks go to James Parr and Frank Sheppard with Apache for encouraging me and supporting me through my work. I would also like to thank Michael Ashby and Brian Coffee for the great discussions and insights.

I would like to thank my committee chair, Dr. Tice, for his guidance and wisdom throughout this project. I would also like to thank my committee members, Dr. Herbert, and Dr. Laya for their direction and insights.

Finally, my deepest love and gratitude goes out to my husband for his patience, support, and encouragement while pursuing my work and to my daughter Natalie for her patience and love.

TABLE OF CONTENTS

Page

LIST OF FIGURES

Page

LIST OF TABLES

Page

1. INTRODUCTION

The Lower Cenomanian Maness Shale is primarily an organic-rich mudstone that locally sources Woodbine and Austin Chalk reservoirs. It is currently being tested as a self-sourcing reservoir which produces oil, condensate, and gas. Since 2008, industry activity has focused on exploiting the Eagle Ford Formation in south Texas as an unconventional reservoir and is now beginning to turn its attention across the San Marcos arch to the stratigraphic equivalent in east Texas. Because industry activity was focused to the southwest, little work was done to understand the depositional controls on source rock variability and distribution within the western East Texas Basin.

The goals of this study are to analyze geochemical signatures, both organic and inorganic, within the Maness Shale in order to test the hypotheses that (1) the organic-rich facies were deposited under anoxic to euxinic conditions that favored the preservation of organic material, (2) the condensed section within the Maness Shale is the most organically enriched zone and primary source rock facies, (3) the carbonate sediments within the condensed interval are biogenic carbonate composed of calcified fossil tests, (4) the association of higher carbonate content with higher TOC is due to higher rates of productivity which may have caused periods of anoxia, and (5) controls on organic matter enrichment varied over time depending on productivity, detrital input, and levels of anoxia.

Chemostratigraphy uses elemental geochemistry including major, minor, and trace elements to subdivide the apparent homogeneity of mudstones (Tinnin et al., 2013). Changes in elemental geochemistry indicate variations within the depositional environment; these changes are used to divide the Maness and Pepper succession into chemostratigraphic packages. Major elements such as Al, Si, Fe, and Ca are used to determine stratigraphic changes in mineralogy (facies) while redox-sensitive trace elements such as Cu, Ni, V, Mo, and U are used to determine depositional conditions (Tinnin et al., 2011).

This study utilizes elemental data from 2 cores from the Maness and Pepper Shales within the east Texas basin. Elemental composition and its distribution from X-Ray Fluorescence (XRF) measurements, bulk source rock attributes from programmed pyrolysis using the Source Rock Analyzer (SRA) and Leco TOC, mineralogy from Fourier Transform Infrared Spectroscopy (FTIR) measurements, and thin sections will all be used as part of this study.

1.1 Objective

The main objective of this research is to determine the mechanisms of enhanced carbon burial during the deposition of the Late Cretaceous Maness Shale by understanding the relationship between organic productivity, carbonate sedimentation, clastic input, burial history, and oxygen levels. Identifying the processes that controlled the deposition and preservation of organic material will aid in understanding the vertical and lateral heterogeneity observed within the source rock facies. Establishing a chemostratigraphic zonation within a stratigraphic framework will allow for better

prediction of the distribution of organic-rich facies within the basin. This objective will be achieved by measuring bulk elemental concentrations within the Manes and Pepper Shales from two cores located in the western portion of the East Texas Basin. Core samples will also be scanned and element distributions mapped across the face of the core samples using an X-ray fluorescence microscope. This will allow us to determine the elemental concentrations and distribution within the rock in order to estimate the redox state of the water column by looking at concentrations of redox-sensitive elements (Cu, Ni, V, Mo, and U). Productivity rates will be estimated by looking at elements which serve as productivity indicators such as P and Ba.

Identifying the relationship between levels of productivity, the redox state of the water column, burial history, and associated sediments will allow us to determine what depositional processes controlled the formation of organic rich facies within the Maness Shale. Plotting TOC with various elements will allow us to determine which elements correlate best to TOC and will give us insight into the depositional process. Lithology will be determined from XRF and FTIR measurements and also compared to TOC levels to determine the relationship between lithology and TOC.

1.2 Study Area

The study area is located in Burleson and Brazos Counties (Figure 1) which lie on the western shelf of the East Texas Basin. Apache Corporation began a pilot program in 2008 testing the Maness/Pepper succession as a potential unconventional resource to be exploited by horizontal drilling and fracking. As part of the program, 3 pilot wells

were drilled down to the Buda formation at varying maturities within Burleson County. The deepest well encountered mechanical issues and they were unable to retrieve core through the entire Maness/Pepper succession. The two shallower cores were drilled further updip and are used in this study.

The interval between the Buda Limestone and Austin Chalk in east Texas varies stratigraphically from what is observed in the Eagle Ford play area in south Texas (Hentz and Ruppel, 2010). Most if not all of the Eagle Ford Formation was eroded within the western portion of the East Texas Basin due to uplift and erosion caused by the rise of the San Marcos Arch (Hentz and Ruppel, 2010). Instead, two other formations comprise the section between the Austin Chalk and Buda Formations which are the Pepper Shale of the Woodbine Group which unconformably underlies the Austin Chalk and the Maness Shale which unconformably overlies the Buda Limestone (Figure 2). The Maness Shale is more carbonate-rich and contains higher amounts of organic material than the overlying Pepper Shale which is more clay-rich with lower carbonate and organic content.

The East Texas Basin is a mature oil and gas province that produces from numerous reservoirs with many styles of traps (Wescott and Hood, 1994). Within the study area, production has historically been from fractured carbonate reservoirs such as the Austin Chalk and Buda Limestone. Eagle Ford Formation siliciclastics, which are locally known as the Sub-Clarksville, produce from sandstone reservoirs which are preserved within incised valleys in the paleo-Brazos River valley (Adams and Carr,

2010). These sediments produce oil and gas in Aggieland Field near the town of Bryan (Adams and Carr, 2010). The Maness/Pepper Shales are the primary source rock for the hydrocarbons produced from these reservoirs (Wescott and Hood, 1994).

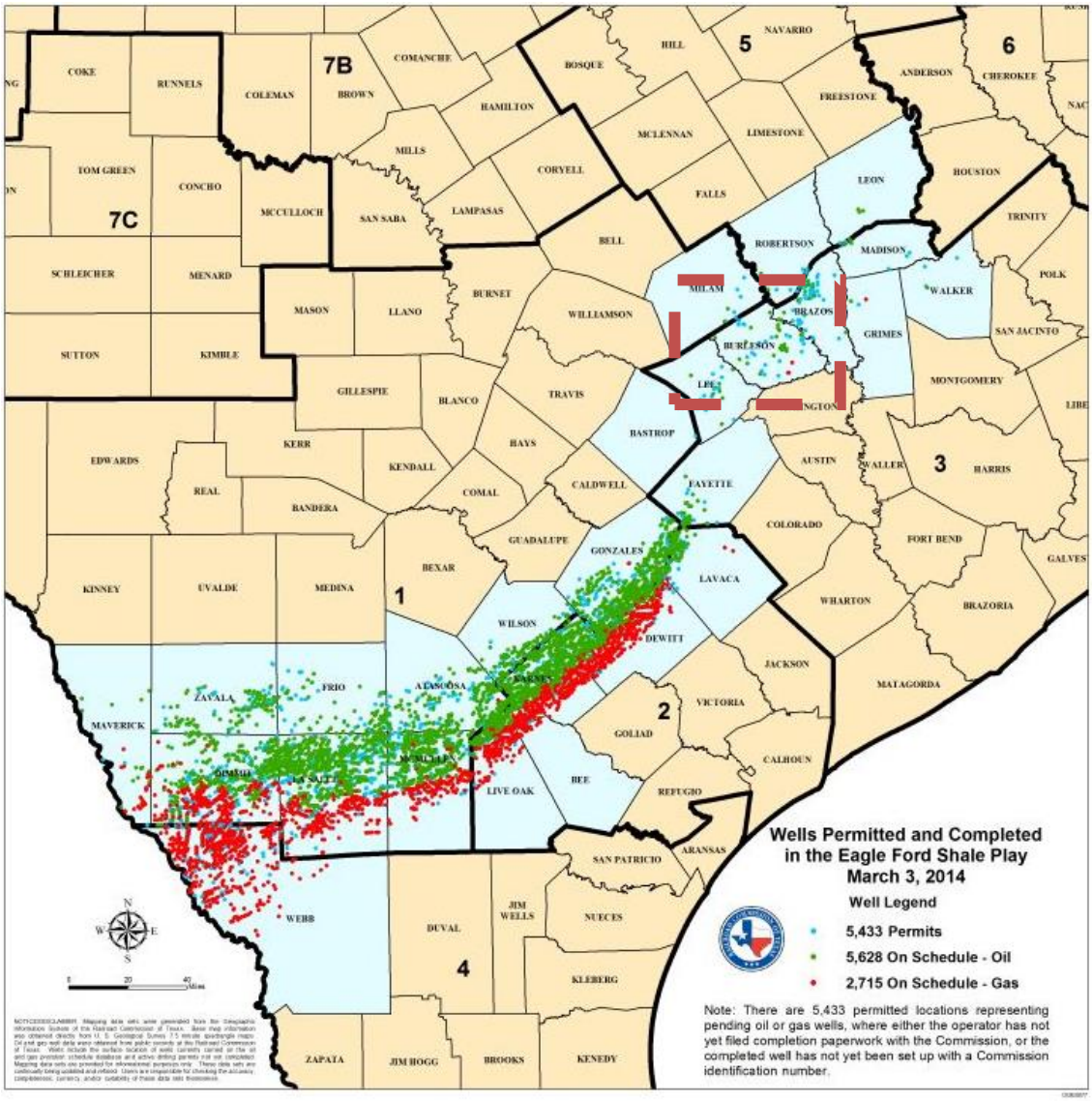

Figure 1: Map of the Eagle Ford play trend. Modified from Railroad Commission of Texas (2014). Study area is outlined in red.

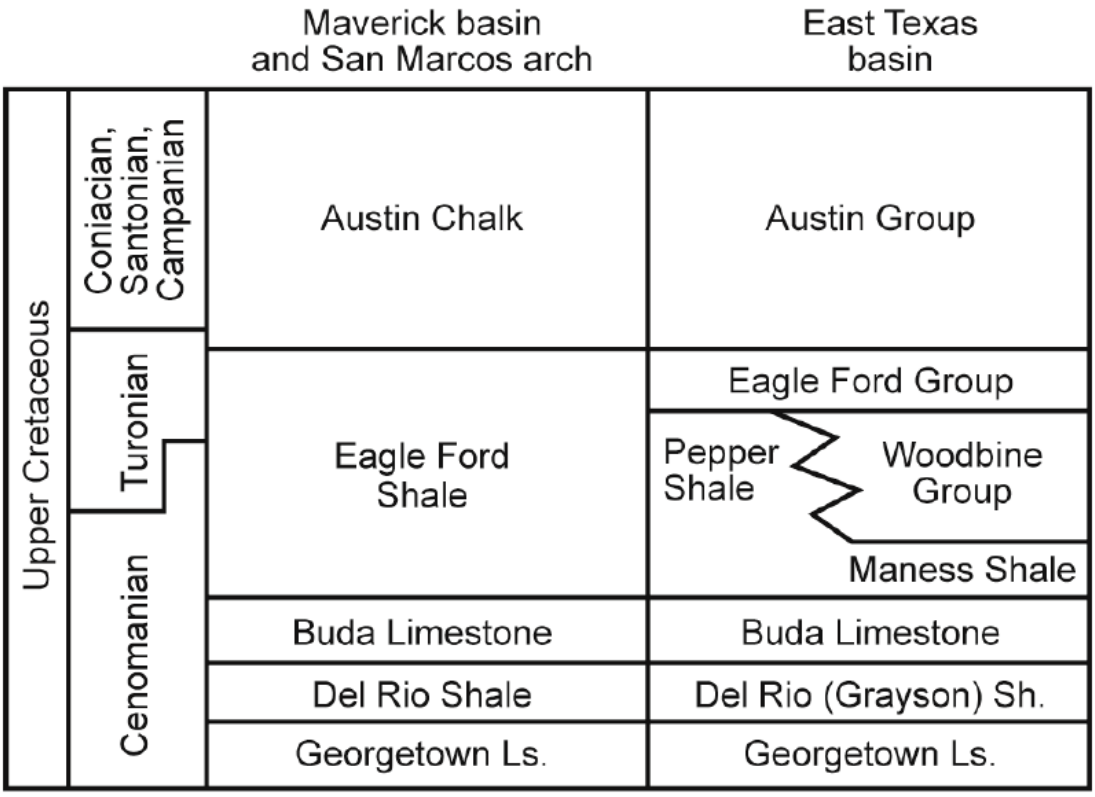

Figure 2: Lithostratigraphy of the Eagle Ford Section across the San Marcos Arch. After Childs et al, (1988), taken from Hentz and Ruppel (2010).

1.3 Geologic Background

The Maness Shale was deposited during the late Cretaceous on the southern end of the Western Interior Seaway which was a marine depositional basin across central North America for almost 50 m.y. (Sageman and Arthur, 1994). The Western Interior Seaway formed as a result of extensional tectonism which was dominated by rifting during the late Jurassic and most of the early Cretaceous (Elder and Kirkland, 1994). A combination extensional tectonics, load-induced subsidence, and large eustatic sea level fluctuations caused the basin to be flooded by a series of marine transgressions from the

Albian to Maastrichtian time (Sageman and Arthur, 1994). Cretaceous sedimentation was largely affected by active tectonism and sea level fluctuations which affected local and regional depositional patterns.

The East Texas Basin is one of a series of extensional basins associated with early rifting located along the onshore Gulf Coast which were actively subsiding depocenters during the Mesozoic and Cenozoic (Mancini, 2008). These localized features formed as a result of tectonic compression from the west in Mexico and the southwestern United States during the Laramide orogeny (Adams and Carr, 2010). The East Texas Basin is a structural embayment bounded on the north and west by the Mexia-Talco fault system, the Angelina-Caldwell flexure to the south, and the Sabine uplift to the east (Ambrose et al., 2009).

The organic-rich Maness Shale is constrained within the western portion of the East Texas basin within a smaller sub-basin known as the Brazos Basin, extending from Houston and Trinity Counties in the northeast to the San Marcos Arch on the Fayette/Gonzales County boundary to the southwest. The Brazos Basin was restricted from open ocean circulation bounded by the Sligo-Edwards shelf to the south and the San Marcos Arch to the west. Shallow lagoons formed on the eastern side of the San Marcos Arch where there were clear shallow waters and limited clastic influx (Adams and Carr, 2010).

The Manes Shale was deposited during a regional transgression across the East Texas Basin under primarily anoxic conditions (Charvat and Grayson, 1981). Anoxic

conditions favored the preservation of oil-prone material within the Maness sediment. These conditions prevent scavengers from consuming the organic matter as well as limiting the downward transport of oxidizing agents (Katz, 2005). There were however periods of oxygenation within the water column as indicated by the presence of normal benthic fauna which show that anoxia was not constant throughout Maness deposition (Dawson, 2000).

The Eagle Ford Formation of south Texas was deposited during a "worldwide oceanic anoxic event" (OAE II) which occurred during the Cenomanian/Turonian (Dean and Arthur, 1998). The slightly older Maness Shale of east Texas was not deposited during the time of OAE II but rather during a smaller, earlier anoxic event that occurred as a result of rapid sea level rise, basin restriction, and irregular topography (Adams and Carr, 2010) . These conditions resulted in the formation of locally stratified basins into which organic material was deposited and preserved. This rapid rise in sea level and irregular topography may have also caused upwelling of nutrients onto the shallow shelf which lead to an increase in productivity, higher levels of anoxia, and deposition of biogenic carbonate.

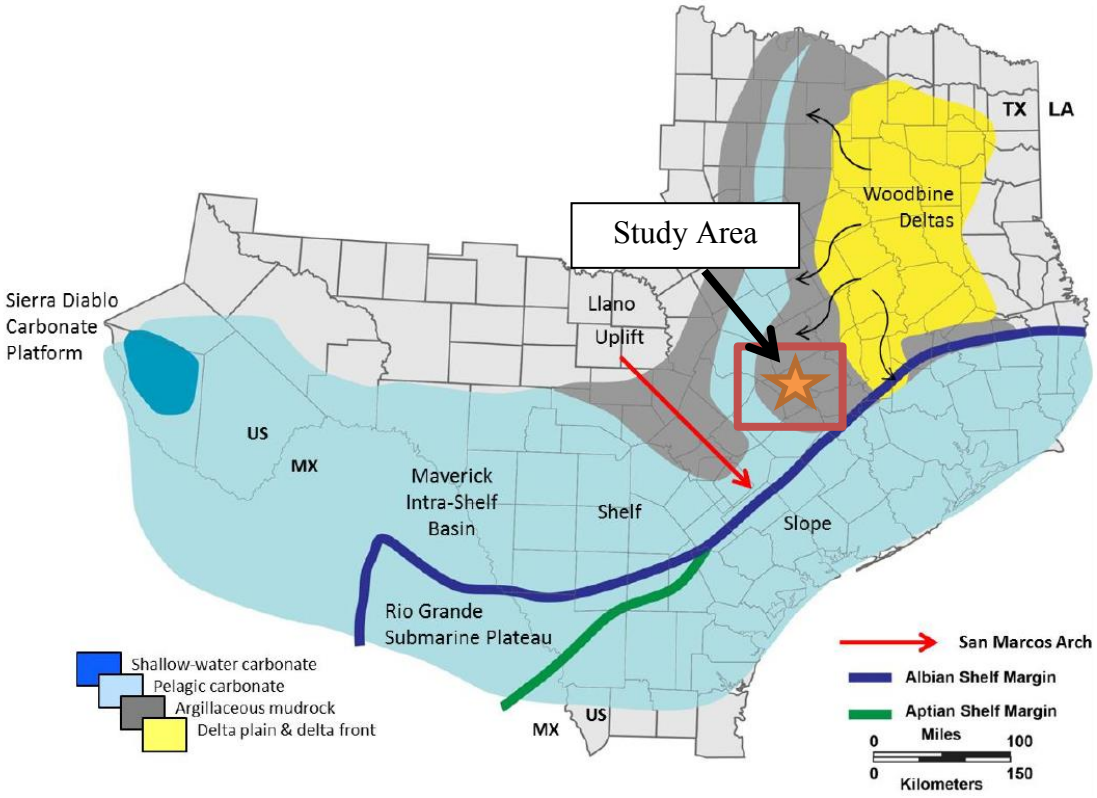

Figure 3: Upper Cretaceous depositional systems during deposition of the Eagle Ford Shale in SW Texas and the Maness/Woodbine interval in East Texas. After Frebourg et al. (2013), modified from Breyer et al. (2013).

Depositional systems during the early part of the upper Cretaceous are shown in figure 3. Sedimentation in the western portion of the East Texas Basin was dominated by pelagic carbonate and argillaceous mudstone deposition (Breyer et al., 2013). In the eastern portion of the basin, delta systems deposited siliciclastic sediments which shed from the ancestral Ouachita mountains and the Sabine Uplift (Hentz and Ruppel, 2010).

Paleotopography largely affected deposition of the Maness and Woodbine sediments. The Sabine Uplift to the east is a positive structural feature which originated

in the late Mesozoic (Ambrose et al., 2009). The Sabine Uplift was active during Maness/Woodbine deposition and clastics were shed from the uplift to the southwest into the basin. Regional cross sections show the majority of the clastics were shed during Woodbine deposition as evidenced by thick accumulations of clastic sediment up to 890' thick in the center of the basin (Ambrose et al., 2009) (Figure 4). The sandy Woodbine facies grade into a prodelta mudstone facies to the SW known as the Pepper Shale. The Maness Shale is also affected by clastic deposition grading from a sandy mudstone in the eastern part of the basin to a more organic-rich calcareous mudstone to the southwest. This unit is characterized in the southwest by a higher gamma ray signature than the overlying Pepper Shale.

The San Marcos Arch on the western edge of the East Texas Basin is another structurally positive feature that influenced deposition of the Eagle Ford/Woodbine/Maness system. It is a broad southeast-plunging structure which divides the Rio Gande Embayment to the southwest from the East Texas Basin (Halbouty, 1966). The San Marcos Arch was a subtle positive feature during the Mesozoic as indicated by thinning of the Maness/Woddbine inteval toward the southwest and over the arch.The relationship of the Eagleford/Maness/Woodbine succession over the arch is unclear as indicated in figure 4 and further work needs to be done to understand the stratigraphic relationsip of these intervals from southwest to northeast.

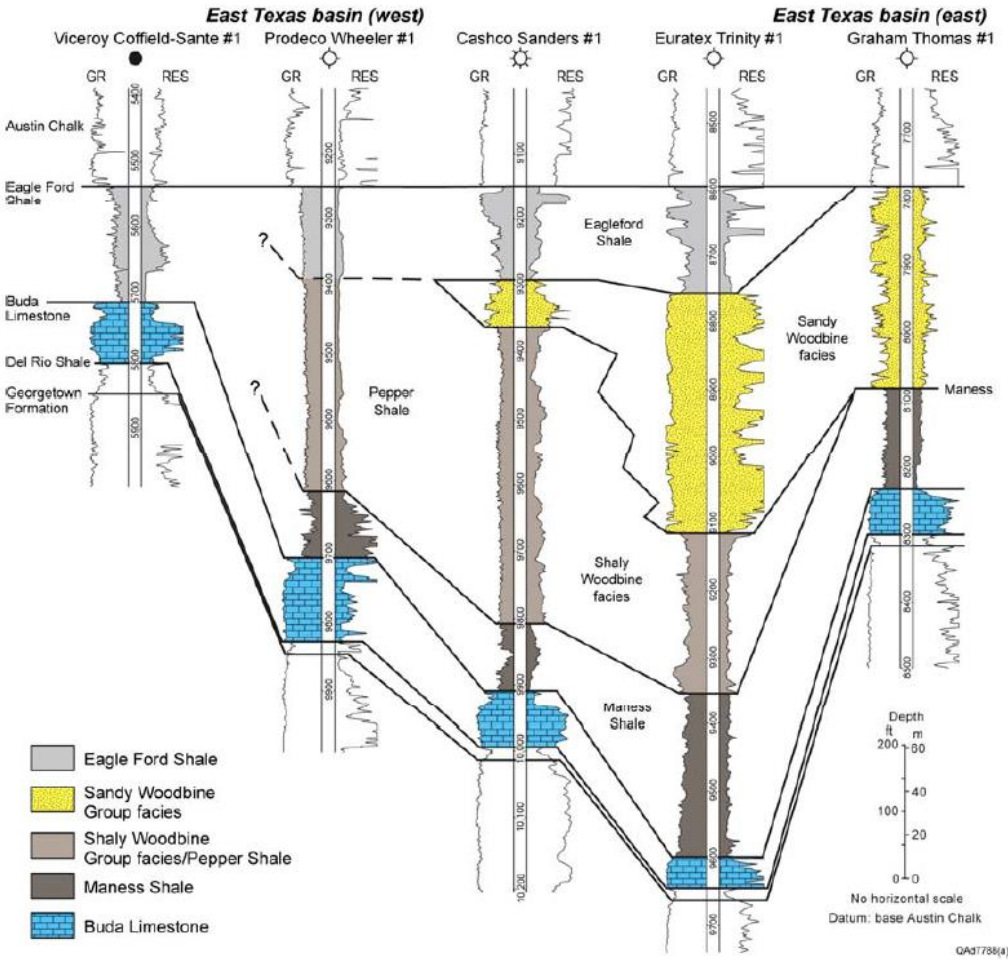

Figure 4: Southwest to northeast stratigraphic cross section on regional strike through the East Texas Basin. Thickening of the Woobine section is evident in the center of the basin while the overall interval from Austin Chalk to Buda thins toward the San Marcos Arch to the SW and toward the Sabine Uplift to the NE. Modified from Hentz and Ruppel (2010).

1.4 Paleoredox and Paleoproductivity Proxies

Insight into how organic-rich mudstones form under varying depositional conditions can be gained by looking at the enrichment of geochemical proxies including redox-sensitive trace elements to determine the oxidation state of the water colmn at the time of deposition. Determining the redox conditions in a marine environment typically

means determining whether conditions were oxidizing or reducing (Tribovillard et al., 2006). Redox-sensitive elements include molybdenum (Mo), vanadium (V), nickel (Ni), copper (Cu), and uranium (U). Redox-sensitive elements are more soluble under oxic conditions and less soluble under reducing conditions which leads to enrichment under oxygen-depleted conditions (Tribovillard, 2006). The determination of paleoredox conditions is used to determine whether the conditions during sedimentation were oxidixing or reducing. The state of oxidation grades from oxic, suboxic, anoxic, to euxinic (Tribovillard, 2006). Oxic refers to oxygen-rich bottom waters, anoxic refers to oxygen-poor bottom waters, and euxinic refers to oxygen-poor waters where free H_2S is present in the water column (Tinnin et al., 2013).

Mo and V are useful trace elements to determine paleoredox conditions due to their low detrital sources making authigenic processes the dominant sources of these metals in sediments (Tribovillard, 2006). Mo concentrations in marine sediments are mainly controlled by the benthic redox state with maximum enrichment occurring under anoxic to euxinic conditions in environments with high organic matter deposition and poor water circulation (Rowe et al., 2009). The combined use of U, V, and Mo enrichment levels can allow the determination of the oxidation state of the water column distinguishing between suboxic to anoxic-euxinic environments (Tribovillard, 2006). Figure 5 shows the relationship of Mo, Ni, Cu, V, and U enrichment as a function of the redox levels in the depositional environment.

Ni and Cu are deposited in the sediment in association with organic matter (OM) making them excellent proxies for TOC (Tinnin et al., 2013). High enrichment of Ni and Cu indicate that there were high levels of OM being deposited which brought these to the sediments and that there were anoxic conditions which preserved them in the sediments (Tribovillard, 2006). In this study, these two elements have the closest correlation to measured TOC. Because of the association of Ni and Cu to organic material, they are good indicators of original presence of organic material while U, V, and Mo are good indicators of paleoredox conditions (Tribovillard, 2006). Ni and Cu also behave as micronutrients being removed by plankton growth and being deposited with the settling organic debris in the upper part of the oceanic water column (Calvert and Pedersen, 1993).

Elements barium (Ba) and phosphorous (P) are typically used as paleoproductivity indicators however they are soluable under reducing conditions and therfore lost from oxygen-poor sediments (Tribovillard, 2006).

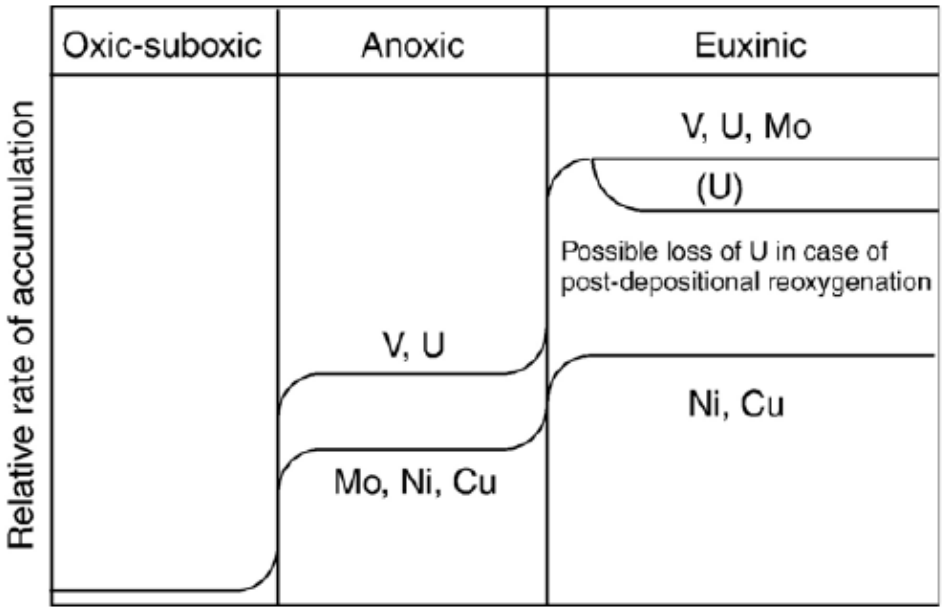

Figure 5: Redox levels determination from Mo, Ni, Cu, V, and U. After Algeo and Maynard (2004), taken from Tribovillard (2006).

2. METHODS

2.1 Core Preparation

The core data set used for this study is summarized in table 1. Cores from two wells drilled in Burleson County, Texas were provided by Apache Corporation each roughly 270' in length containing the full Maness/Woodbine succession from the top of the Buda to the base of the Austin Chalk. Both wells contain a full logging suite which was run by Baker Hughes and was depth shifted to match the gamma ray log response from the cores. Core samples from each core were used for XRF analysis, FTIR mineralogy determination, SRA pyrolysis/TOC, and to create thin sections. Cores were described and classified according to the work done by Workman and Grammer (2013) on cores from the south Texas Eagle Ford Shale.

Well Name	Field	County	Well Type	Depth (ft.)	Core (ft.)
Well "A"	Giddings	Burleson, TX	Oil	7,974'- 8244.5'	270.5'
Well "B"	Giddings	Burleson, TX	Oil	8,980'-9,249'	269'

Table 1: Core from the Pepper and Maness Shale used for this study.

2.2 Thin Sections

Thin sections were prepared from core chips throughout the Eagle Ford succession from each core to assist in determination of facies type. Thin sections were prepared by TPS Enterprises, LLC in Bellaire, TX. Standard 1" X 2" samples with a 15 micron finish were prepared and impregnated with blue fluorescent dyed epoxy as well as total carbonate staining which includes Alizarin Red and Potassium Ferricyanide. Alizarin Red will allow for detection of calcite within the sample while Potassium Ferricyanide will assist in detection of iron. The samples will be studied and photographed using plane polarized light, cross polarized, and reflected light.

2.3 Fourier Transform Infrared Spectroscopy (FTIR)

Mineralogy was determined from FTIR measurements conducted by graduate students at the "Integrated Core Characterization Center" at University of Oklahoma as part of a mudrock consortium. Sixteen minerals can be identified through FTIR measurements and include quartz, calcite, dolomite, siderite, aragonite, illite, kaolinite, smectite, chlorite, mixed clay, oligoclase, feldspar, albite, pyrite, apatite, and anhyrdrite. Measurements were taken throughout each core and used to determine the lithology and rock types within the Maness and Pepper Shale cores.

2.4 Source Rock Analyzer/TOC/Visual Kerogen Analysis including Vitrinite Reflectance

Core samples for SRA programmed pyrolysis, LECO TOC, and Visual Kerogen Analysis (VKA) including Vitrinite Reflectance (%Ro) measurements for both wells

was sent to Weatherford Laboratories in Shenandoah, TX. Resultant data including TOC, Hydrogen Index, Oxygen Index, oil potential (S2), maceral type (VKA), and %Ro were used to determine the organic content, type, and maturity. This data was also used to determine kerogen types within the Maness and Pepper Shales.

Three core samples from well "B" were analyzed for vitrinite reflectance thermal maturity (%Ro). There was good organic recovery for visual study in all 3 samples although vitrinite material was sparse and the recommended 40 vitrinite particle samples could not be obtained in 2 of the samples.

2.5 X-Ray Fluorescence (XRF) Methods

Core chips were taken every 5' and analyzed by Chemostrat, Inc. in Houston, TX for whole-rock elemental data. Major elements are reported as a percentage while minor trace elements are reported in ppm. The bulk elemental data was converted to a digital .las file and plotted against the wireline logs in the PETRA CrossSection Module to compare elemental data to wireline log responses. Chemostratigraphic zones were determined from changes in elemental concentrations for each well. These zones were used to help determine depositional changes within a sequence stratigraphic framework that was devised based on gamma ray and resistivity logs from multiple wells across the study area.

Selected core samples were also scanned by x-ray fluorescence (XRF) microscopy on a Horiba XGT-7000 X-Ray Analytical Microscope. This allowed determination of elements present through fluorescence peak analysis and mapping of

the elemental distributions across the face of the core sample. The XRF data was used to estimate the redox state of the water column, determine distribution of sediments and sediment types within the succession, and to divide the section into chemostratigraphic packages based on overall changes in the rock chemistry and sedimentary features.

2.6 ImageJ Methods

Element maps were made using Image J software in order to identify mineral types and distribution within a core sample. A Fast Fourier Transform (FFT) was applied to Fe maps in order to identify sedimentary features in otherwise massive looking samples. The element Ca was used to determine carbonate content within the samples and Fe and S was used to determine the redox state at the time of deposition.

3. RESULTS AND DISCUSSION

3.1 Chemostratigraphic Zonations

A chemostratigraphic zonation through the Maness/Woodbine sequence was determined by using changes in key elements and elemental ratios which indicate changes in facies and depositional environment. Eight chemostratigraphic packages were identified in each well (Figures 6 and 7). These zones were correlatable between the two study wells with similar changes seen in the bulk elements which define each zone (Figure 8).

Zones were defined by changes in major, minor, and trace elements. Major elements Ca and Al were used to determine facies changes defining more carbonate rich zones from more argillaceous zones. A terrigenous index curve was calculated by summing Al+Si+K+Na+Ti and used to determine the relative amount of detrital sediments within each zone (Figures 9 and 10). Redox-sensitive trace elements U, V, Ni, Mo, and Cu were used to determine the oxidation state of the water column within each zone (Figures 11 and 12).

Facies seen throughout the cores from both wells range from laminated argillaceous mudstone to laminated inoceramid and foraminiferal Wackestone (facies 1-5) as described by Workman and Grammer (2013) in south Texas Eagle Ford cores. The bulk of the mineralogy seen within the zones is clay (primarily illite) and carbonates (primarily calcite). Lesser amounts of quartz, albite, anhydrite, and apatite are also

present. Fauna seen in all zones are dominantly composed of globigerinid foraminifera with lesser amounts of inoceramid fragments.

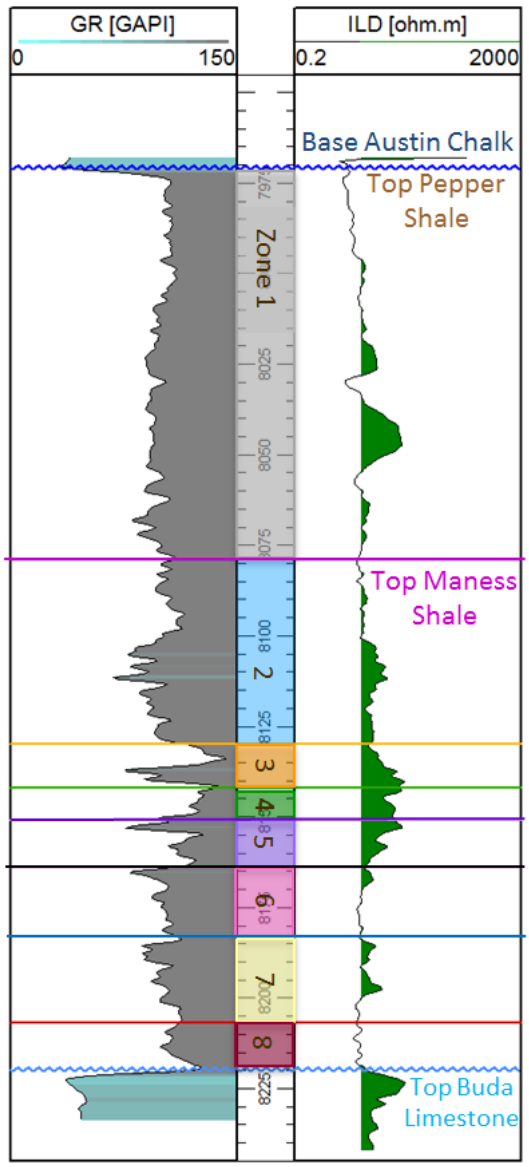

Figure 6: Chemostratigraphic zonations for well A.

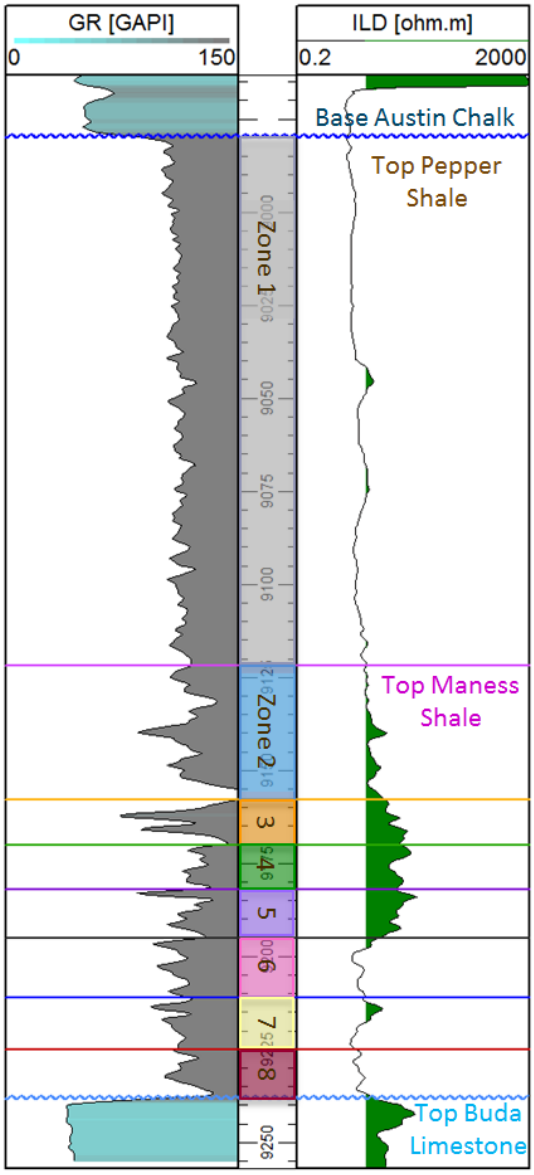

Figure 7: Chemostratigraphic zonations for well B.

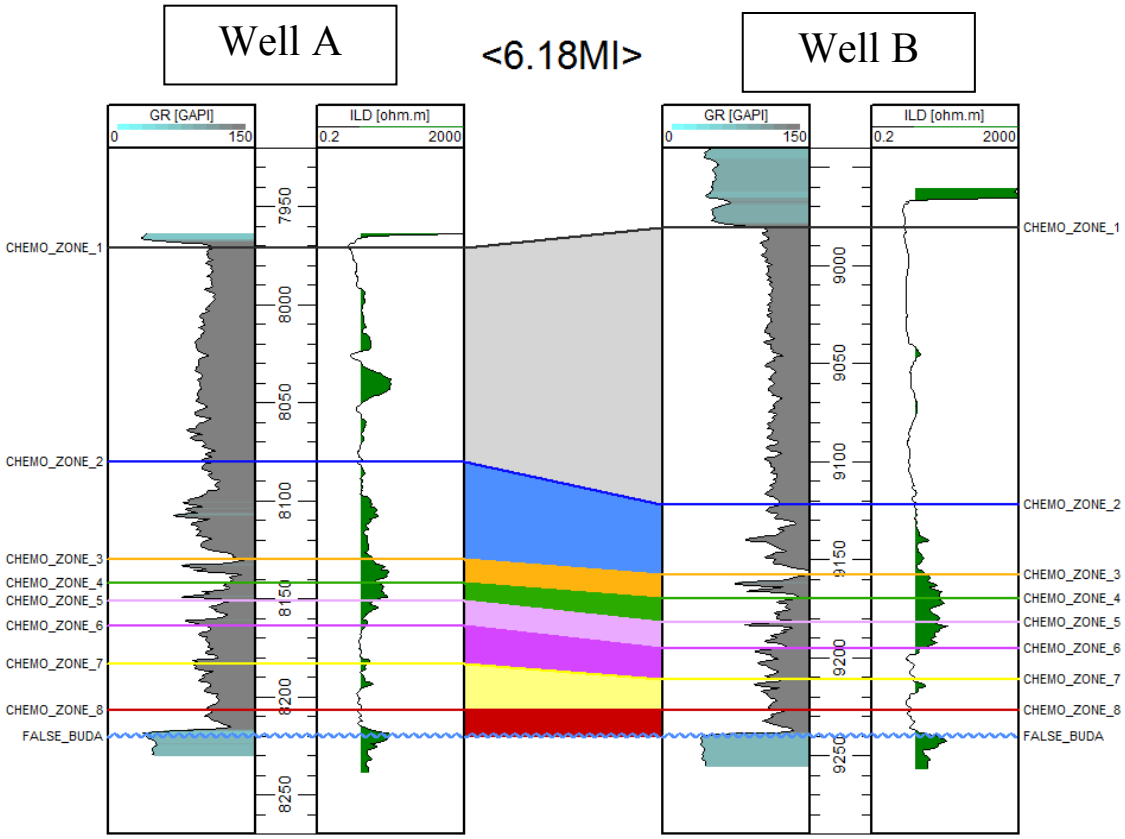

Figure 8: Correlation of chemo zones between the two study wells. TOC is plotted to show more organic rich zones.

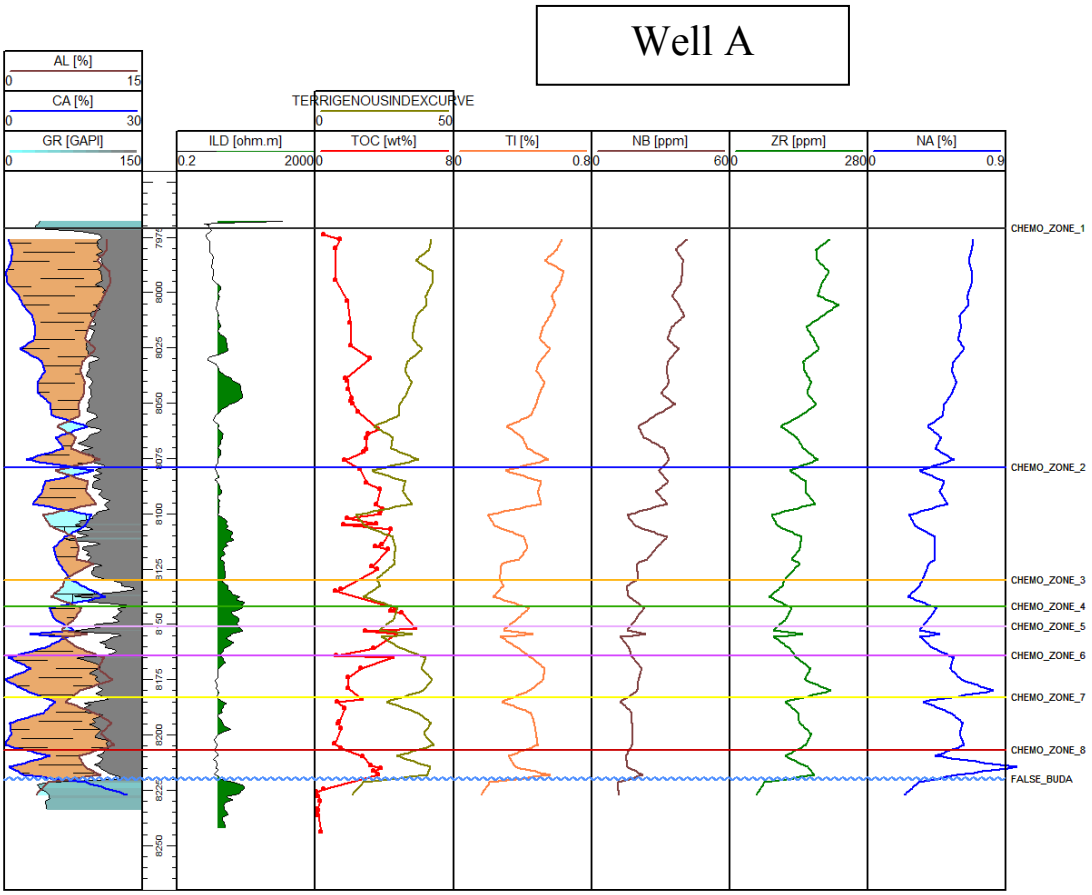

Figure 9: Major and minor elements used as detrital indicators used in part to define chemo zones for well A.

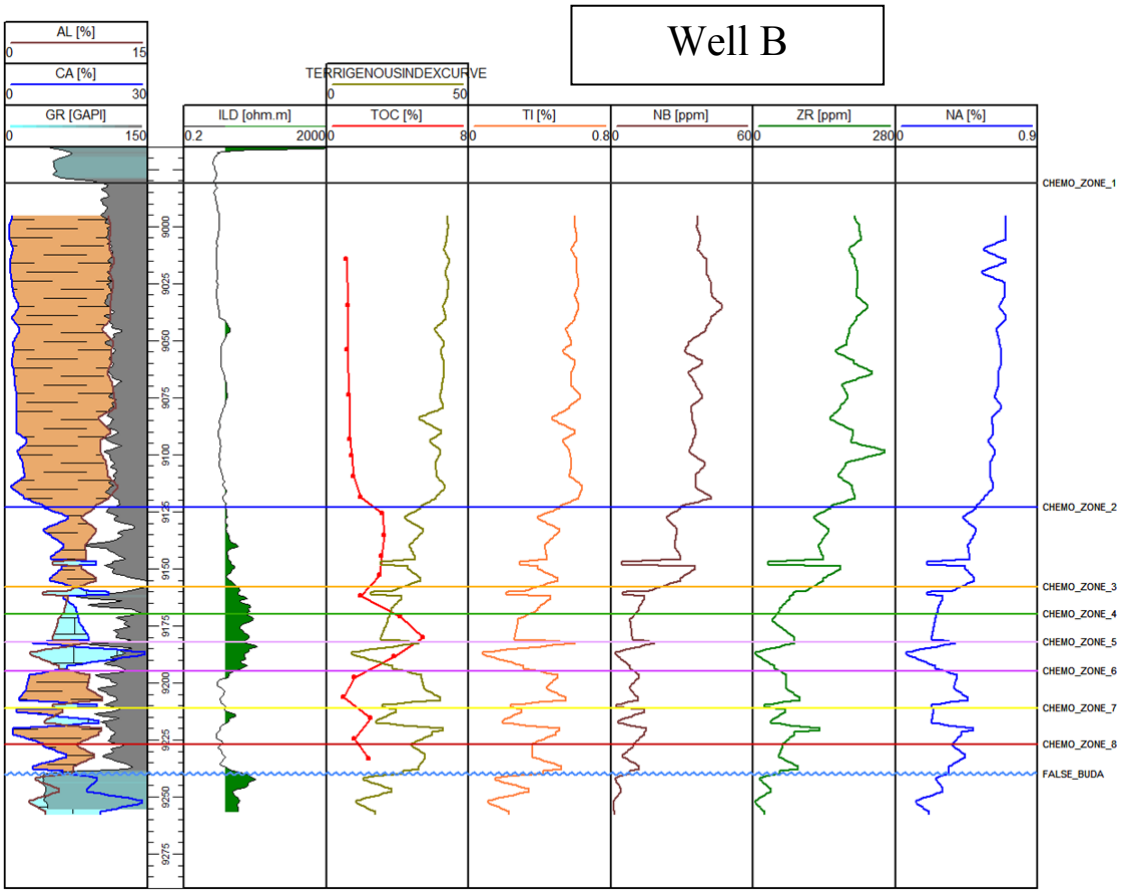

Figure 10: Major and minor elements used as detrital indicators used in part to define chemo zones for well B.

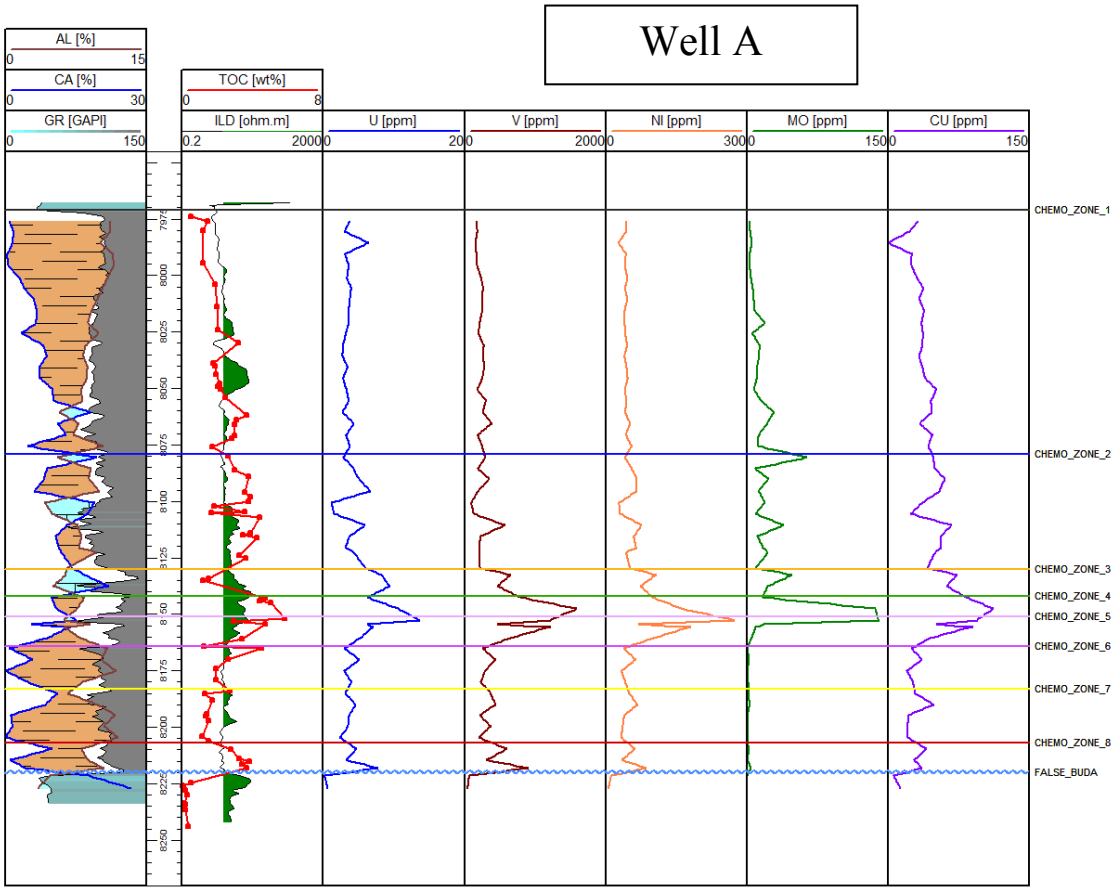

Figure 11: Redox-sensitive trace elements used to determine oxidation levels in the water column for well A.

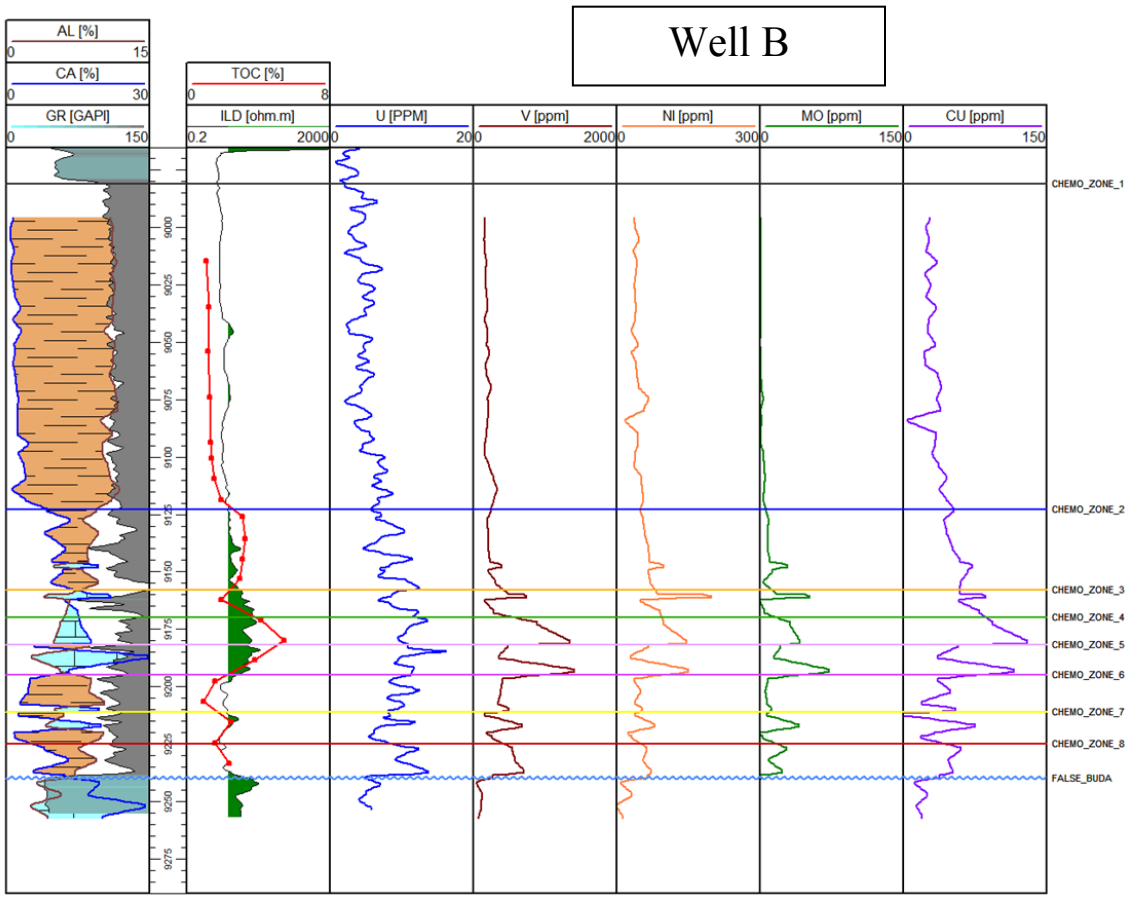

Figure 12: Redox-sensitive trace elements used to determine oxidation levels in the water column for well B.

3.1.1 Zone 1

Zone 1 is entirely located within the Pepper Shale of the Woodbine Formation. The Pepper is primarily an argillaceous mudstone containing high levels of Al as well as Ti and Nb which most likely reside in illite. FTIR mineralogy measurements show that illite is the dominant clay mineral in the Pepper Shale averaging 35.9% of the 65% total clay volume in well A and 36.8% of the 72.8% total clay volume in well B. Carbonate content averages 14.3% and 7.6% for well A and B respectively and is predominantly

biogenic calcite in origin. The terrigenous curve is high throughout zone 1 indicating a high level of detrital sedimentation at this time. This is confirmed by regional stratigraphy which shows the Pepper Shale was deposited on the distal prodelta shelf as Woodbine clastics were shed from the northwest and prograded into the East Texas Basin (Adams and Carr, 2010). Sediments being deposited are primarily clay rich, quartz averages less than 3% in this zone in either well. Siderite is also present averaging 7% in both wells.

Redox-sensitive elements are low through zone 1 indicating oxic to suboxic conditions prevailed during the deposition of the Pepper Shale (Tribovillard et al., 2006). TOC within zone 1 averages 3% (Ro 1.0) in well A and 1.7% (Ro 1.2) in well B. These are present day TOC measurements which are lower today than when they were initially deposited due to conversion to oil or gas (Jarvie 1991). Visual kerogen analysis performed by Weatherford on a core sample from 9086.9' from well B indicates there has been moderate alteration to the kerogen as determined by recycled/oxidized vitrinite. This confirms that the TOC present within zone 1 was poorly preserved due to more oxygenated conditions and is therefore has lower generative potential. The plot in figure 7 shows that the terrigenous curve and TOC are inversely related indicating organic matter dilution from the influx of detrital sediment into the basin.

The primary facies seen in core through zone 1 is a thinly laminated argillaceous mudstone as shown in figure 13. Core samples are highly fissle breaking easily along bedding planes due to the high clay content. Laminations are composed of globigerinid

foraminifera and are wispy and wavy throughout indicating occasional reworking by winnowing currents (Workman and Grammer, 2013). Thin sections show that forams are often filled with clay. Measurements from a thin section from well B at a depth of 9,060' (Figure 13) show that clay filled forams make up approximately 2.05% of the total area shown. Calcite content is low measuring 0.66% of the total thin section area and is found around the rim of foram tests. Pyrite is abundant measuring 4.42% of the total area and also fills all or part of the forams. Reflected light shown in figure 13(c) is used to detect pyrite which is abundant in the sample. Pyrite averages 1.4% in both wells A and B ranging from 0-12% in total volume.

3.1.2 Zone 2

Zone 2 corresponds to the upper portion of the Maness Shale which is bounded at the top by an unconformity. This unconformity can be seen by a dramatic decrease in P and Ba which are both productivity proxy elements (Tribovillard et al., 2006). A rapid increase in calcium is seen with a corresponding rapid decrease in detrital indicators Al, Ti, Rb, and Th. The same elemental changes are present in both wells at the top of zone 2 as well as at another sequence boundary within the Maness at the top of zone 7 and at the sequence boundary at the Maness/Buda contact.

Zone 2 is the transition from more oxic/suboxic conditions dominated by clastic deposition within the Pepper Shale to more anoxic conditions with lower amounts of detrital influence in the Maness Shale. The levels of Ca increase while Al decreases indicating an increase in carbonate deposition.

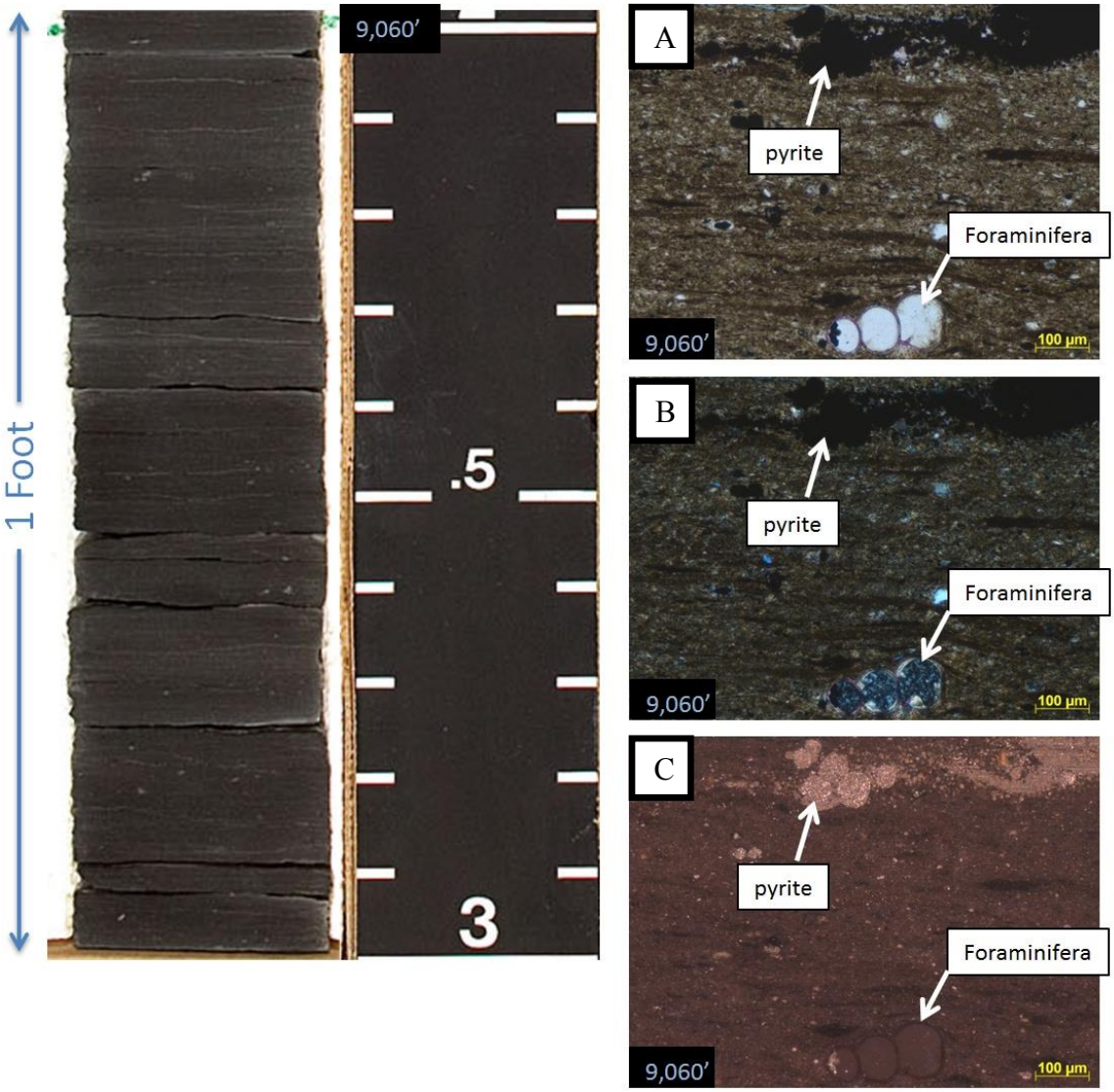

Figure 13: Core and thin section photographs from zone 1 in well B. Thin section photographed in plane polarized light at 100x (A), cross polarized light at 100x (B), and reflected light at 100x (C).

The terrigenous index curve decreases from the high levels seen in zone 1 but is still higher relative to deeper zones. Fluctuations are seen in the levels of Ca and Al indicating periods of increasing and decreasing detrital input.

Clay content is still dominantly composed of illite which averages 22.4% of the 42.6% total clay volume for well A and 17.7% of the 47.2% total clay volume for well B. Carbonate content for well A averages 35.5% of which 31.7% is composed of calcite and 3.9% dolomite. Carbonate content for well B averages 31.8% of which 26% is calcite and 5.8% is dolomite. Dolomite is as high as 41% in some samples. Pyrite levels are low averaging less than 1%. Quartz is also low averaging less than 2% in both wells. Siderite makes up 8% and 10% of the bulk volume in wells A and B respectively.

Redox-sensitive element levels begin to increase slightly from what is measured in zone 1 but remain relatively low indicating oxic to suboxic and at times anoxic conditions prevailed during this time. Fluctuations in these elements are seen in both wells and indicate fluctuating levels of oxygenation. TOC also shows an increase through zone 2 averaging 3.9% in well A and 3.1% in well B. Well B contains similar TOC to well A which is less mature indicating this zone in well B may have originally been more organic rich.

Observed facies in zone 2 are laminated argillaceous mudstone to weakly laminated calcareous foraminiferal mudstone. An increase in carbonate content can be seen in the core through zone 2 as a more massive mudstone that is less fissle than what is observed through zone 1. The primary carbonate allochems are globigerinid foraminifera with lesser amounts of disaggregated inoceramids while some zones show abundant fine crystalline ferroan dolomite as seen in thin sections in figure 14. The Ferroan dolomite makes up 16% of the thin section shown in Figure 14. In areas of

abundant ferroan carbonate, calcite content is low making up roughly 1.6% of the thin section area. Pyrite is also low making up roughly 1.1% of the area.

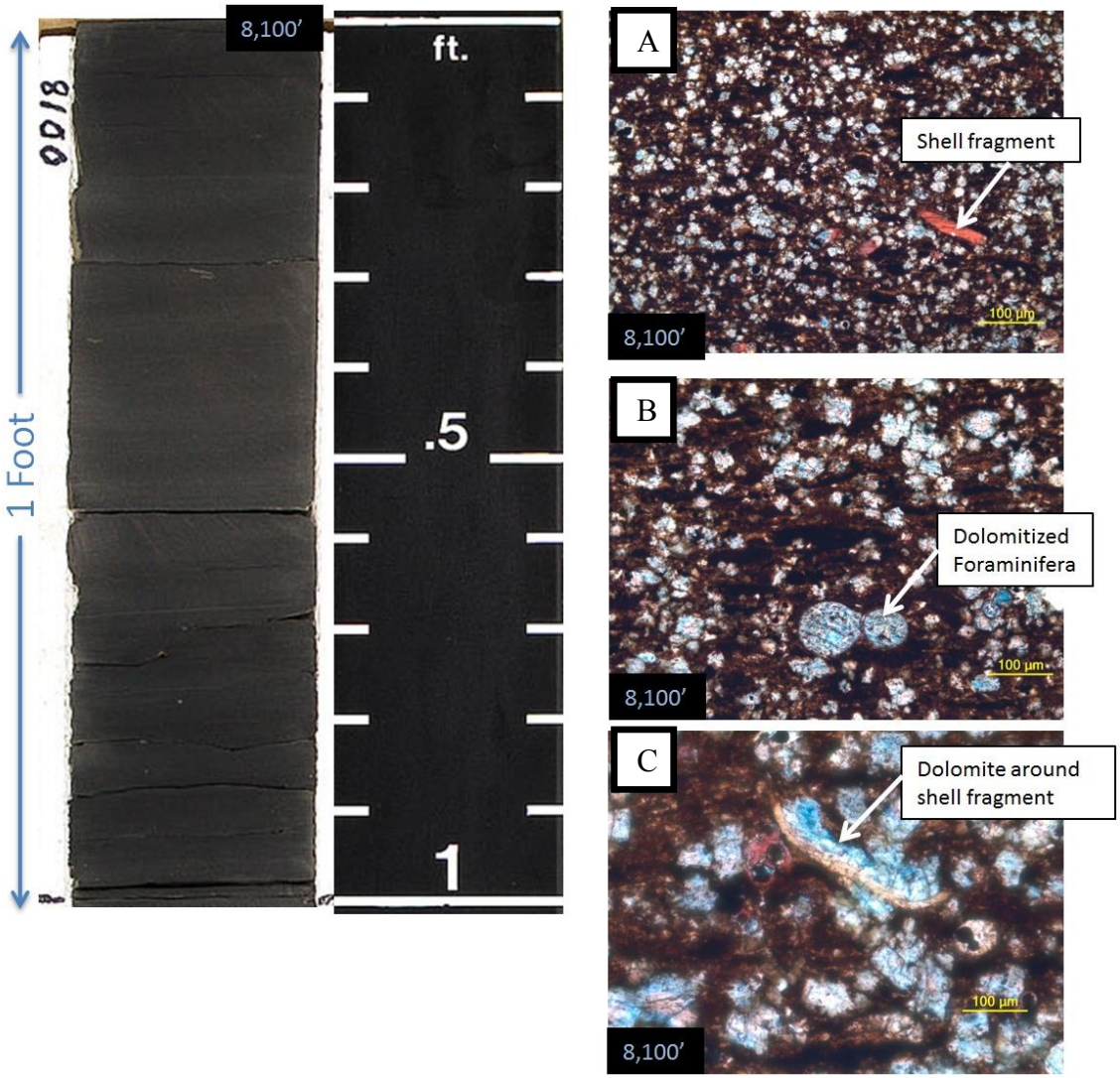

Figure 14: Core and thin section photographs from zone 2 in well A. Thin sections photographed in plain polarized light at 100x (A), plane polarized light at 200x (B), and plane polarized light at 400x (C).

Ferroan carbonate is clearly replacive as seen by forams which have been fully replaced and precipitation around shell fragments in thin sections. The dolomite can form as magnesium is released during smectite conversion to illite in argillaceous mudstones (Zeng and Tice, 2014).

3.1.3 Zone 3

Zone 3 is the top of the condensed section which is composed of zones 3, 4, and 5. It is bounded on the top by a maximum flooding surface which can be seen by an increase in Ca as well as redox-sensitive elements Mo, Ni, V and Zn. Flooding surfaces contain thin hemipelagic to pelagic sediments as the shelf is starved of terrigenous sediments (Van Wagoner et al., 1990). A sharp drop in the terrigenous index curve at the top of the section as well as a sharp drop in other detrital indicators such as Al, Ti, and Nb confirms a depositional environment with low detrital input. Ca content increases sharply at the top of zone 3 and corresponds to a regionally continuous gamma ray marker known informally as the “rabbit ears”. Calcium is derived from biogenic carbonate composed of inoceramid fragments and abundant forams. Total carbonate content in zone 3 is high averaging 44.5% in well A and 50% for well B. A few samples contain dolomite as high as 11% of the total sample volume. Clay content is dominantly made up of illite and averages 38.5% for well A and 32.1% for well B.

Redox-sensitive elements show a large increase at the top of zone 3 in association with the condensed section then drop quickly throughout the rest of the section. High Ca and high levels of redox-sensitive elements at the top of the zone

indicate that during this time of maximum regional transgression, there was a great abundance of fauna which may have caused oxygen depletion in the water column. TOC is overall low in this zone, averaging less than 2% although neither well had a TOC measurement at the exact same depth as the high Ca and redox zone which may have the highest TOC in the zone.

Core through zone 3 (Figure 15) shows an abundance of fossiliferous laminations and is interpreted as the laminated inoceramid and foraminiferal Wackestone. Laminations are random and wavy indicating higher bottom water energy as evidenced by disturbed bedding seen in core and thin section. Thin section photos show the fossil rich beds composed of benthonic inoceramid fragments and globigerinid foraminifera. The fragments of inoceramids are highly disturbed and broken indicating they were transported under higher energy conditions and not in life position. Abundant mud rip up clasts also attest to the higher energy environment that prompted the transport of these fauna. Workman and Grammer (2013) interpret this facies to be deposited in an oxygen deficient subtidal environment where periods of higher energy interrupt quieter background sedimentation. Vertical fractures are abundant and indicate an increase in brittleness as a result of the high amount of calcite in this section.

Carbonate is clearly abundant in this zone as seen in thin sections in figure 15. Calcite makes up 21.1% of the total thin section area while ferroan carbonate makes up only 0.3%. Calcite is seen partially to fully replacing foram test as well as inoceramid fragments. Clay is also seen replacing foram tests which make up 1.8% of the total area.

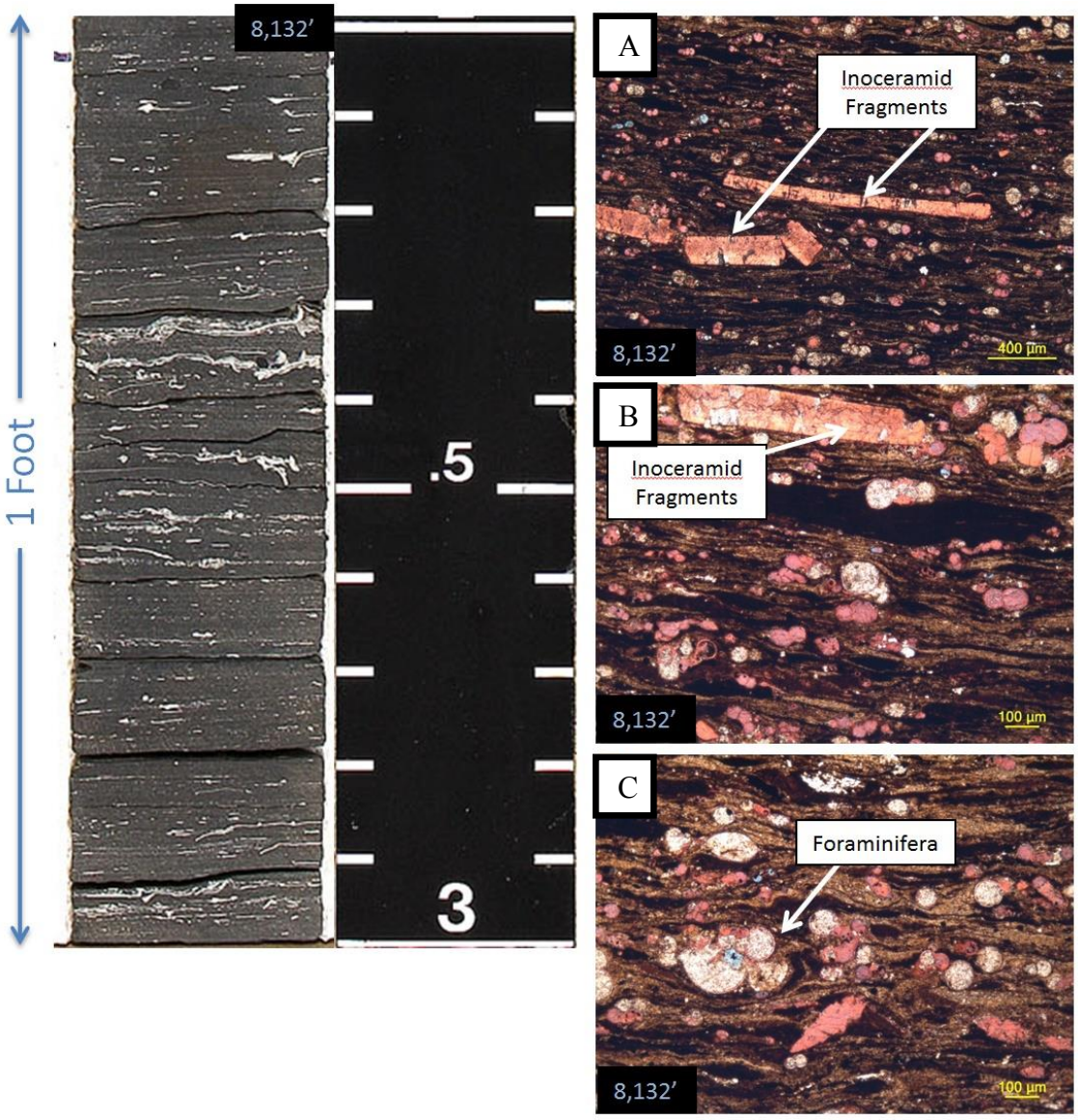

Figure 15: Core and thin sections from zone 3 in well A. Thin sections photographed in plane polarized light at 50x (A), plane polarized light at 100x (B), and plane polarized light at 100x (C).

3.1.4 Zone 4

Zone 4 is located within the organic rich condensed section of the Maness Shale. Oil-prone source rocks such as the Maness are commonly deposited during transgressions within the condensed sequence (Liro et al., 1994). Dark organic rich shales such as seen in zone 4 have lithological, geochemical, and biological characteristics that indicate stagnant, oxic to suboxic conditions (Workman and Grammer, 2013). Redox-sensitive elements N, V, Mo, Cu, and U are very high which confirm anoxic conditions during this time. TOC levels are high and average 4.7% in well A and 4.8% in well B. The terrigenous index curve as well as other detrital indicator elements are low through this zone and indicate little sediment input into the basin. The presence of low oxygen and low sedimentation rates along with high accommodation during maximum flood result in the increased TOC seen within zones 4 and 5 (Creaney and Passey, 1993). The gamma ray and resistivity log profiles are high through this zone which further indicates high levels of organic matter as well as the presence of hydrocarbons.

Three main variables control organic-matter accumulation: rates of production, destruction, and dilution (Passey et al., 2010). It has been determined that rates of destruction were low due to anoxic conditions as determined by high levels of redox-sensitive elements and low sedimentation rates are indicated by low levels of detrital indicator elements. Productivity can be inferred by looking at levels of phosphorous which are high in both wells through zone 4. Primary producers provide organic material

while secondary producers supply brittle carbonate material which allows for better fracability (Passey et al., 2010).

No quartz is measured in either well through this zone; carbonate and clay minerals continue to make up the majority of the section. Clay content through zone 4 averages 48.7% in well A of which 29.2% is illite and 34.4% in well B of which 18.9% is illite. Calcite content is high averaging 33.5% in well A and 43.4% in well B; dolomite is less than 2% in either well. No pyrite is measured in well A while about 2% is measured in well B. Siderite continues to average 6-8% in each well remaining fairly constant through all the zones.

The core through zone 4 is primarily made up of the laminated foraminiferal wackestone facies which is a thinly laminated mudstone with thin planar laminations of bioclastic laminae. The laminae are made up of primarily globigerinid foraminifera. The core samples are black to dark brown and lack benthic fauna which confirms an anoxic to suboxic environment. Forams are observed in thin section as being partially to completely replaced by pyrite which makes up 4.8% of the total thin section area. Clay filled forams are also seen and make up 1.9% of the thin section area. Calcite lines the rim of foram tests and makes up 1.8% of the total area.

The abundance of foraminifera and higher levels of productivity indicators P and Ba indicate increased productivity in the photic zone. There is a lack of bioturbation seen in the core which confirms the depositional environment to be anoxic.

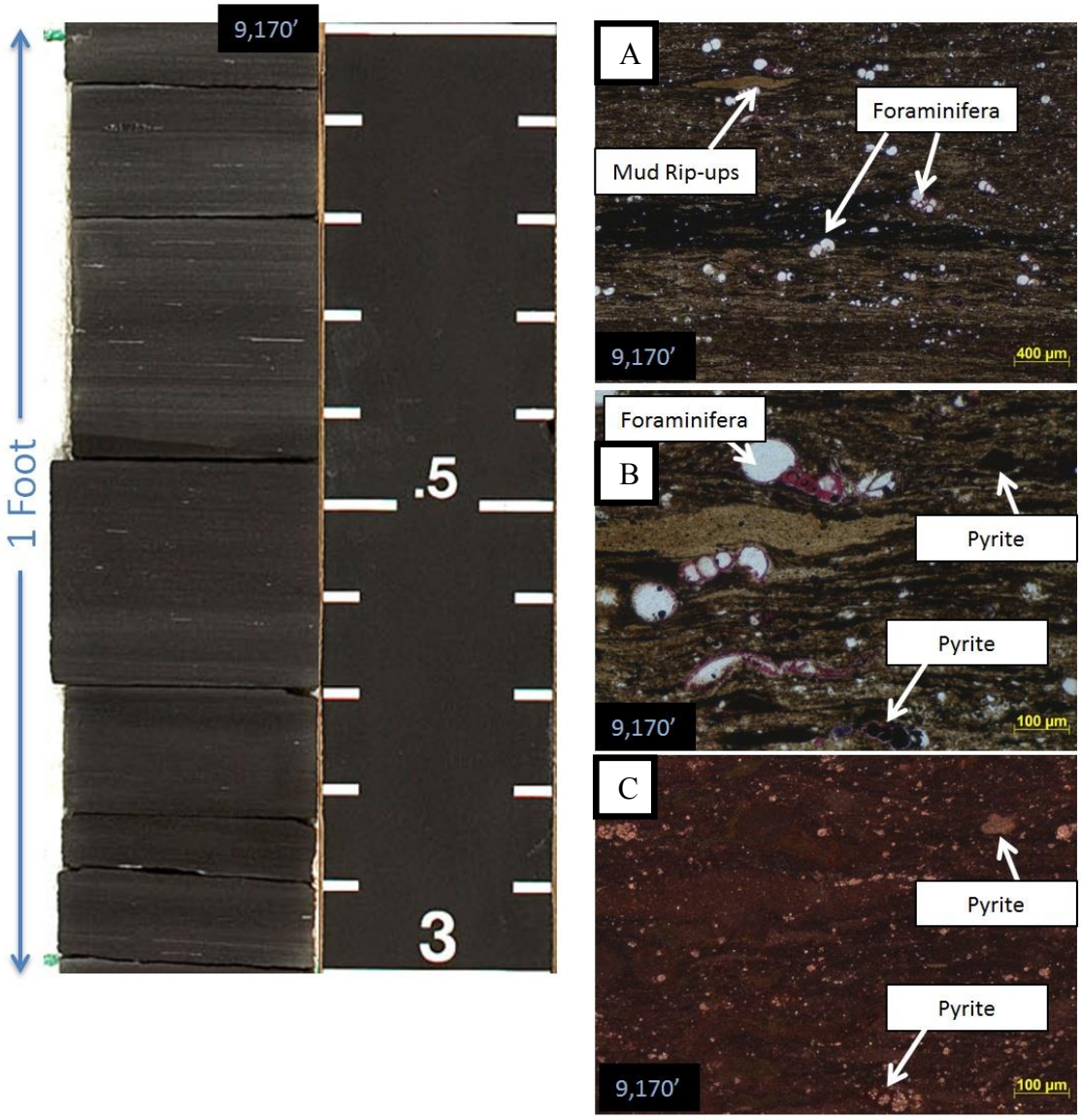

Figure 16: Core and thin sections from zone 4 in well B. Thin sections photographed with plane polarized light at 25x (A), plane polarized light at 100x (B), and reflected light at 100x (C).

3.1.5 Zone 5

Zone 5 is the basal zone within the Maness condensed section. The top of zone 5 is determined by a high Ca and Mg streak which can be seen in logs as a low gamma ray

marker and is correlatable throughout the study area. Similarly to zone 4, it exhibits very high levels of the redox-sensitive elements N, V, Mo, Cu, and U indicating anoxic conditions. Also in common with zone 4 is the low level of detrital input as indicated by the terrigenous index curve and other detrital proxy elements. What is different about zone 5 is the highly elevated level of molybdenum which reaches concentrations as high as 140 ppm in some samples. Enrichment of Mo is related to the presence of hydrogen sulfide (H_2S) in the water column during deposition (Tinnin et al., 2013). The presence of H_2S within the water column under anoxic conditions is known as euxina (Tribovillard et al., 2006). Levels of Mo from 20 to 160 ppm are seen in modern anoxic/euxinic basins such as the Black Sea, Cariaco Trench, Framvaren Fjord, and Saanich Inlet (Tinnin et al., 2013).

TOC is high in zone 5 averaging 4.8% in well A and 3.8% in well B. Illite makes up 30% of the total 49.2% clay in well A and 27.8% of the total 48% clay in well B. Calcite ranges from 3% to 61% in well A and 1% to 64% in well B. Biogenic calcite is the primary source of carbonate through most of the zone however, in some samples a diagenetic carbonate is the primary form of carbonate. An increase in sulfur and iron are seen in this zone which is usually associated with pyrite however, pyrite averages 1% or less in either well.

Zone 5 is also primarily a laminated foraminiferal wackestone as was seen in zone 4. Zone 5 however shows evidence of the diagenetic carbonate cements that can be seen in the core as well as in thin sections as seen in figure 17. In core these zones are

massive grey to crystalline and range in thickness from 2 – 7mm. They occur as thin beds within an organic rich, thinly laminated mudstone to wackestone with gradational to sharp contacts. In thin section, large crystals can be seen replacing sediments as well as fauna which are primarily globigerinid foraminifera and benthic inoceramids. Diagenetic calcite is seen as long bladed to small scattered crystals which make up 58% of the thin section area shown in Figure 17. This diagenetic calcite is interpreted to be early due to the large crystal growth, most likely before the muddy substrate had fully lithified. Siderite makes up 8.5% of the thin section area and can be seen cross cutting the calcite crystals which indicates it is later than the calcite cement. There is no evidence of bioturbation in the zone confirming anoxic to euxinic conditions.

Redox-sensitive elements are slightly reduced within the thin-bedded calcite beds. A sample of one of these beds was taken from well B at a depth of 9,175' and analyzed; it showed very high levels of Ca (29.7%) and Fe (4.3%) with lower than average Mo (15.1 ppm), V (358.8 ppm), and Ni (28.9) as compared to other samples from zone 5. This indicates that formation of these diagenetic calcite beds may not always be tied to euxinic conditions as documented by Kruse (2014) in the South Texas Eagle Ford Shale. On the contrary, high levels of Mo which indicate euxinic conditions are tied to high TOC within this zone. A sample from 8,152' from well A with very high levels of Mo (139 ppm) also measures high TOC (5.23 wt. %).

No TOC data is available from one of the thin bedded, diagenetic calcite beds. However, it appears that there is a small amount of organic material contained in these

beds as seen in thin section but the concentration is low in comparison to the bulk volume of calcite.

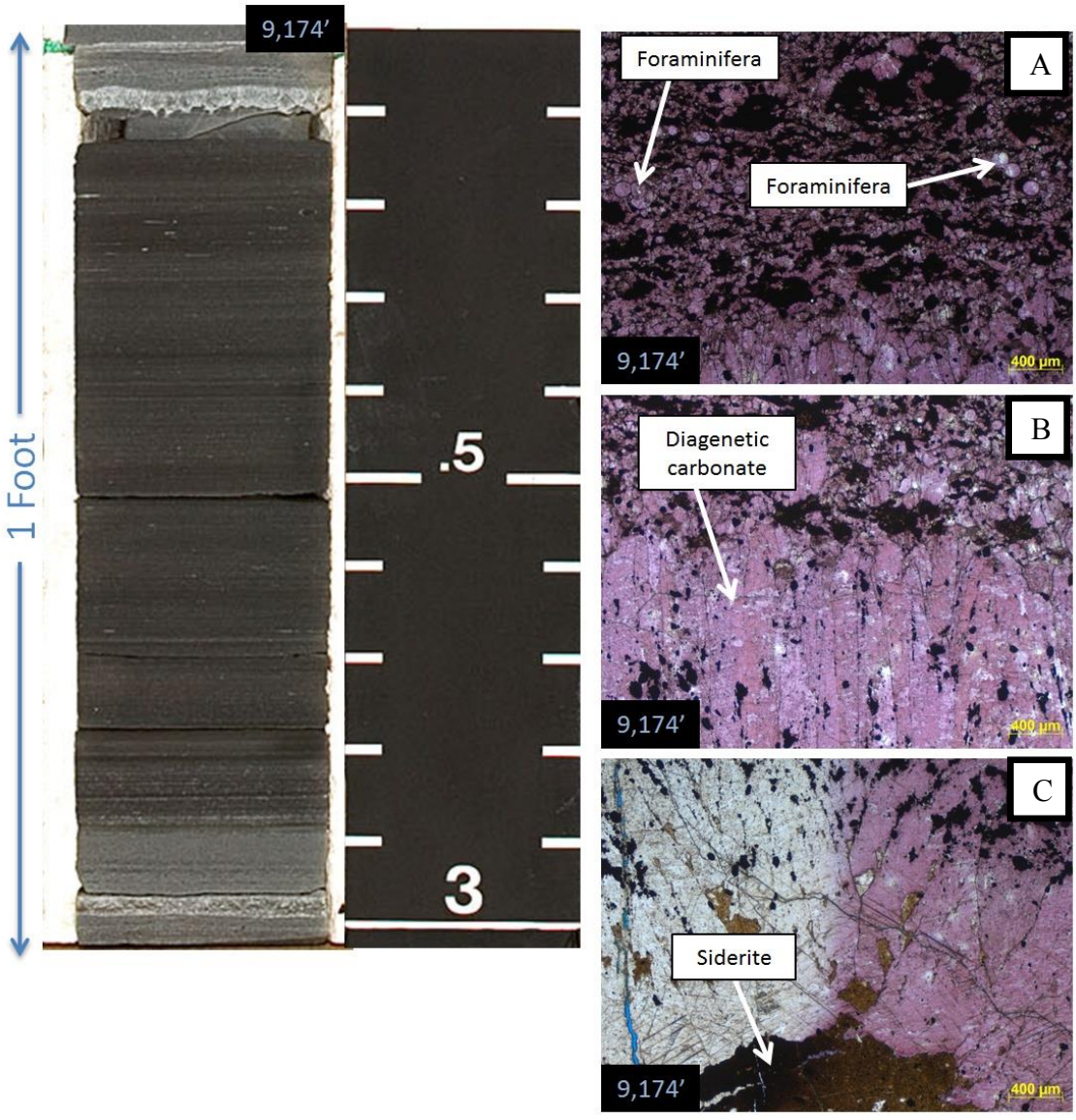

Figure 17: Core and thin sections from zone 5 in well B. Thin sections photographed in plane polarized light at 25x with calcite stain in pink (A), plane polarized light at 25x with calcite stain seen in pink (B), and plane polarized light at 25x with calcite stain on the right side of the slide (C).

3.1.6 Zone 6

Zone 6 sits below the condensed section within the transgressive lower Maness. It is defined by a decrease in Ca with an increase in Al, Ti, and Rb along with a drop in redox-sensitive elements. Carbonate content and TOC fall to very low levels throughout this zone. The terrigenous index curve increases indicating higher detrital input into the basin. Redox-sensitive elements are low indicating oxic conditions prevailed during this time. More oxygenated, higher depositional energy can also be inferred based on the high amount of current induced structures such as ripples seen in the core.

Clays make up 64% of the bulk volume in well A of which 40.4% is illite. Clay makes up 63.9% of the bulk volume in well B of which 37.8% is illite. Carbonate content is low averaging 9.8% in well A and 6.2% in well B. Quartz remains negligible averaging less than 4% in either well. Pyrite is seen in large amounts in some samples ranging from 0-14% with the highest amounts seen in well B. Siderite is 6.2% and 7.4% in wells A and B respectively. TOC is decreases through this zone averaging 2.3% in well A and 1.29% in well B.

Zone 6 is primarily made up of laminated argillaceous mudstone alternating with thin beds of mud lean wackestone (figure 18). Thin sections show these beds are alternating layers of fine grain clastics that contain abundant disseminated pyrite (5.1% of the thin section area) and dark organic carbonate rich layers that contain abundant ankerite crystals (6% of the total thin section area). Calcite is also seen in the dark organic rich layers and makes up 2.9% of the total thin section area.

The transition between the alternating beds is seen as gradational to sharp in thin sections. The fine clastic sediments may represent pulses of detrital sediment being deposited into the basin interrupting the background sedimentation which is the dark organic carbonate layers. In the clastic beds, pyrite is more abundant indicating that iron in the water column is preferentially precipitating to pyrite. In the organic carbonate beds, iron is preferentially precipitating to ankerite which can be seen replacing forams. The formation of ankerite is presumed to be early due to the formation of euhedral crystals and the lack of displacive fabrics.

3.1.7 Zone 7

Zone 7 is bounded on the top by a flooding surface that separates it from zone 6 above. It is similar to zone 6 in that Ca is low and Al is high along with the terrigenous input curve indicating high levels of detrital sedimentation at this time. Redox-sensitive elements are low and correspondingly TOC levels are the low averaging 1.7% in well A and 2.1% in well B. P and Ba levels are low indicating productivity within the basin was low due to a lack of nutrients.

Clays make up 65.4% of the bulk volume of which 40.3% is illite in well A and 56.8% with illite being 35.4% of the clay volume in well B. Carbonate makes up 11.4% of the bulk volume of rock in well A and 21.2% in well B. Quartz is low accounting for 1-4% of the total volume while pyrite contained is 1.75% and 0.9% in well A and B respectively. Siderite averages 6.1% and ranges from 1-12% in both wells.

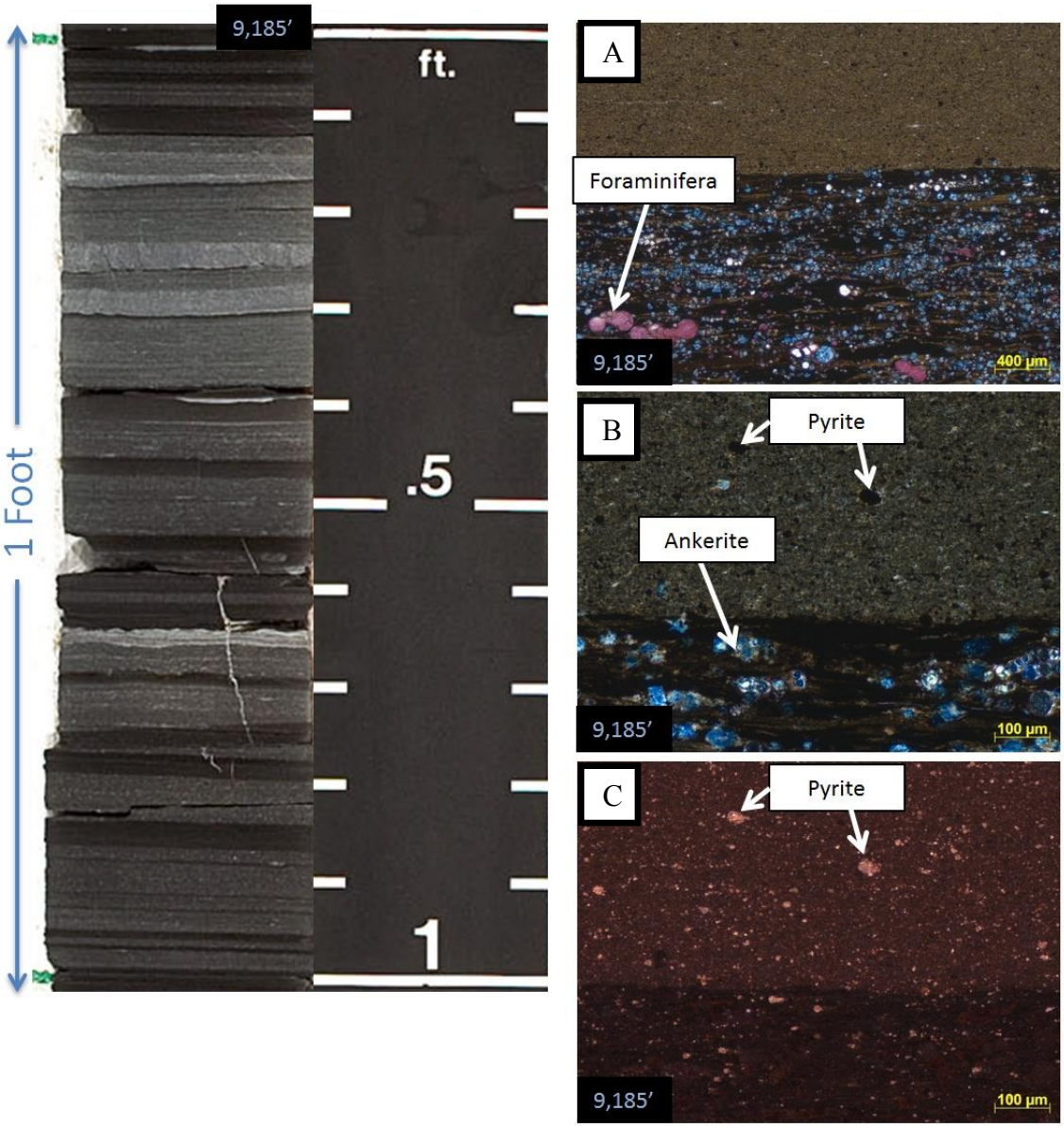

Figure 18: Core and thin sections from zone 6 in well B. Thin sections photographed in plane polarized light at 25x with Potassium Ferricyanide stain shown in blue and calcite stain in pink (A), plane polarized light at 100x (B), and reflected light at 100x (C).

Core through zone 7 primarily shows the laminated argillaceous mudstone facies. The core is fissile with mostly planar laminations with occasional ripple laminations and

scours which appear to be current or gravity induced structures. These structures are medium grey in color and are interstratified within a black to dark brown shaly unit. Thin sections shown in figure 19 are from the interface of zone 6 and 7 which is interpreted to be a flooding surface. At the contact, laminations contain abundant angular quartz grains (21.8% of the total thin section area) with blocky detrital pyrite (9.1% of the total thin section area). The pyrite is coarse and intermixed or layered with layers of quartz grains. These are interpreted to be micro-lags caused by small scale density flows which periodically interrupt the clay rich background sedimentation. Carbonate content with calcite being less than 1% of the total thin section area and ferroan carbonate making up 1.5%.

The pyrite is most likely syngenetic which consists of fine-grained euhedral crystals as seen here as opposed to diagenetic pyrite which usually forms large, spherical framboids (Tribovillard et al., 2006). This distinction in pyrite can help determine the location of the chemocline which is the separation of oxic waters above from anoxic waters below. In this case, syngenetic pyrite forms if the chemocline lies above the sediment-water interface (Tribovillard et al., 2006).

3.1.8 Zone 8

Zone 8 overlays the Buda limestone and is distinguished from zone 7 by the higher redox elements and corresponding higher TOC which averages 3.4% in well A and 1.62% in well B. This is the basal zone of the Maness transgressive sequence where deposition of organic material was high during the initial flooding event.

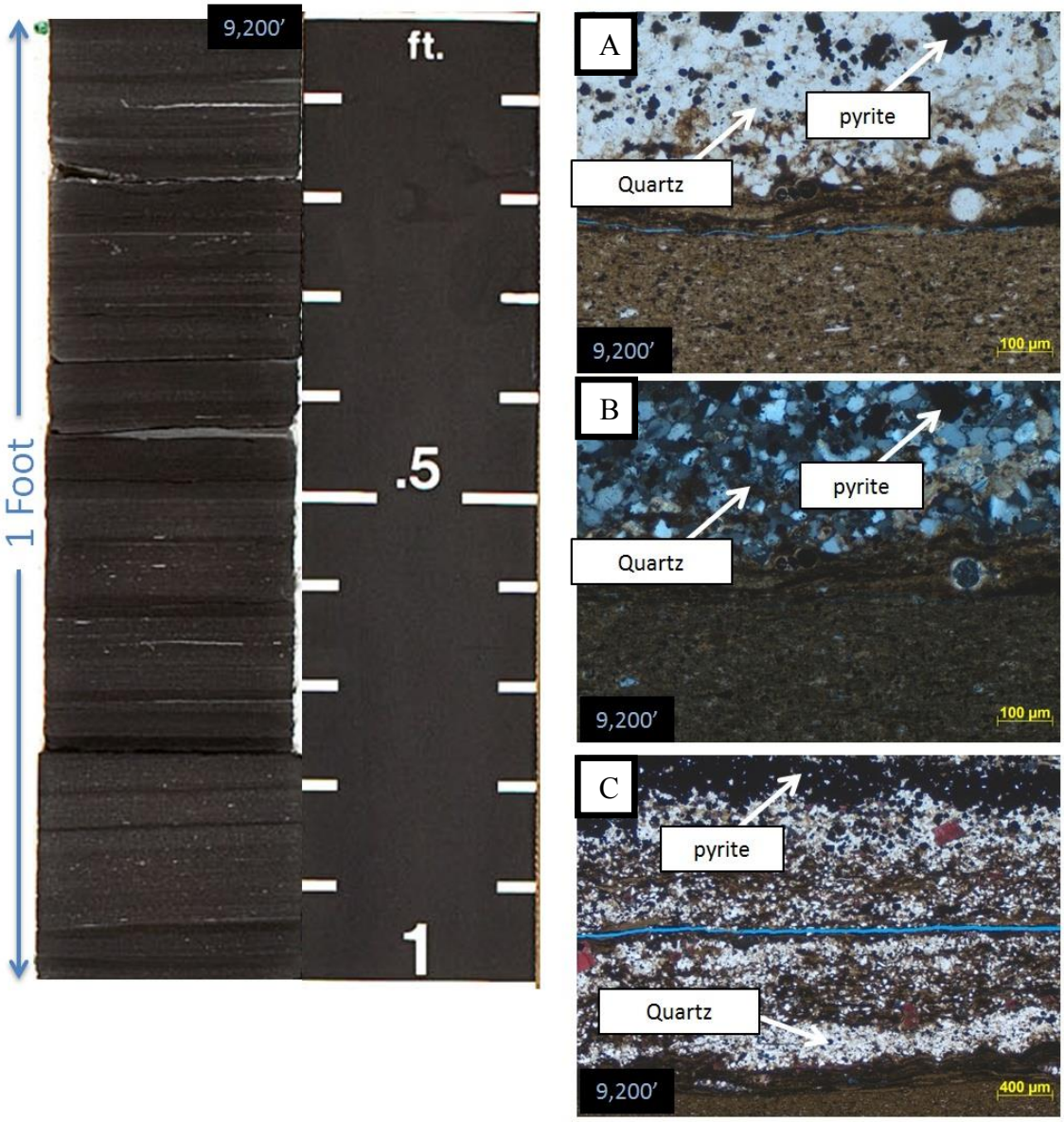

Figure 19: Core and thin sections from zone 7 in well B. Thin sections photographed in plane polarized light at 100x (A), cross polarized light at 100x (B), and plane polarized light at 25x (C).

Marine organic shales such as the Maness often have the high TOC values near their bases (Creaney and Passey, 1993). This unit along with units 4 and 5 within the

condensed section are interpreted to be the richest source rock intervals. Slight increases in P and Ba are seen in some samples within zone 8 and indicate higher levels of productivity.

Clays make up 49.9% of the bulk volume of which 25.6% is illite in well A and 61.9% with illite being 32.3% of the clay volume in well B. Carbonate content increases from what is measured in zone 6 above making up 26% of the bulk volume in well A and 18.8% in well B. Dolomite averages just under 3% in both wells. Quartz averages 1-5% in each well and pyrite averages 0.125% in both wells. Siderite averages just over 8% in both wells.

Core through zone 8 is predominantly laminated argillaceous mudstone. The core is clay rich and fissle with thin planar laminations and is dark brown to black in color. Thin sections show abundant detrital quartz interpreted to be micro-lags caused by small scale density flows similar to what was seen in zone 7. Syngenetic pyrite is present also as seen in zone 7 indicating the chemocline is above the sediment-water interface. A fining upward from the coarse-grained lag to clay rich siltstone can be seen in the sediment grain size and in the size of the pyrite crystals.

Calcite content is low making up 1.6% of the total thin section area and is primarily associated with a small scattering of globigerinid foraminifera. Some forams are cemented with ferroan carbonate which makes up just 0.4% of the total thin section area. Pyrite is abundant and makes up 2.9% of the total area.

The Buda contact is at a depth of 8,219’ and can be seen in figure 20 as a gradational contact from a massive grey limestone below to the dark organic rich Maness Shale above.

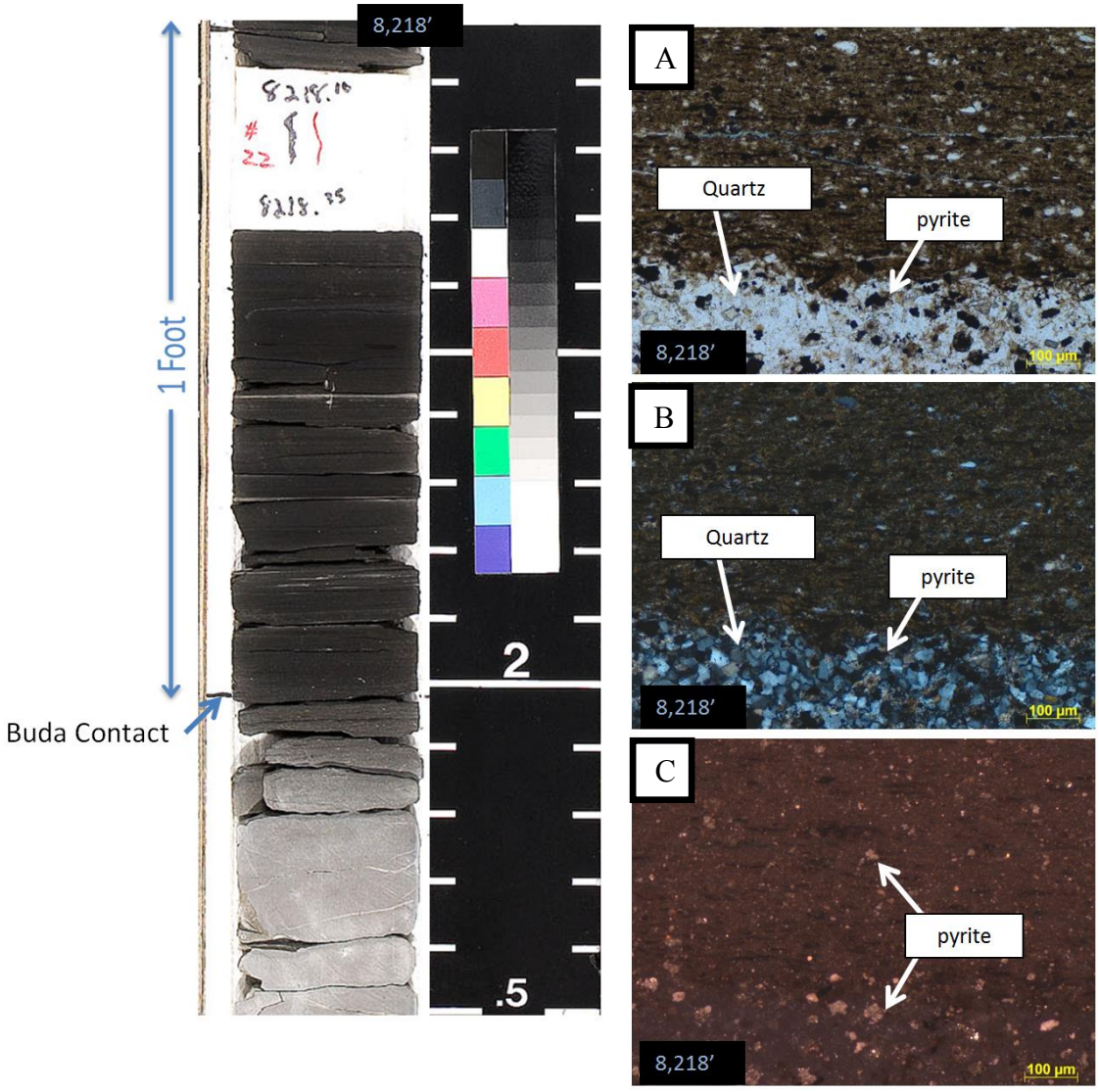

Figure 20: Core and thin sections from zone 8 in well A. Thin sections photographed in plane polarized light at 100x (A), cross polarized light at 100x (B), and reflected light at 100x (C).

3.2 Element Distributions within the Condensed Section

X-ray images were created using the analytical microscope and used to determine element distributions within zones 3, 4, and 5 which make up the organic-rich condensed section within the Maness Shale. This allowed characterization of lithofacies as well as determination of carbonate and pyrite distributions.

3.2.1 Zone 3

Zone 3 contains high levels of Ca with lower concentrations of redox-sensitive trace elements than what are measured in zones 4 and 5. The highest levels of Ca are seen in the low gamma ray streak that is correlatable within the entire study area (Figure 21 A). The abundant Ca is associated with significant amounts of yellow grains which are pyrite. Figure A shows a possible phosphate bone from the high GR marker in well A. Phosphate, high TOC, pyrite, and glauconite are commonly associated with a condensed section (Dawson and Almon, 2010). Just above the high gamma ray marker, a more massive mudstone can be seen at the top of zone 3 (Figure 21 B). The homogenous nature of this sample may be due to higher levels of bioturbation. Faint laminations can be seen indicating this rock may have been deposited as a more laminated facies then subsequently churned up by organisms living in the muddy substrate.

Sample A from well A shows very high concentrations of Ca (22.2%) with lesser amounts of Fe (1.7%) and S (0.6%) as measured by whole-rock elemental analysis. Levels of Mo in sample A are low measuring 22.3ppm while V is moderate measuring 462.6 ppm. Sample B has less Ca (12.6%) with higher levels of Fe (3.2%) and S (1.3%).

Mo is below the level of detection so cannot be measured; V is low measuring 163.4 ppm. TOC measures 1.2 wt. % near sample A and 2.0 wt. % in sample B. Well A may have low TOC due to carbonate dilution while sample B may have low TOC due to more oxygenated conditions as indicated by bioturbation and low redox-sensitive element levels.

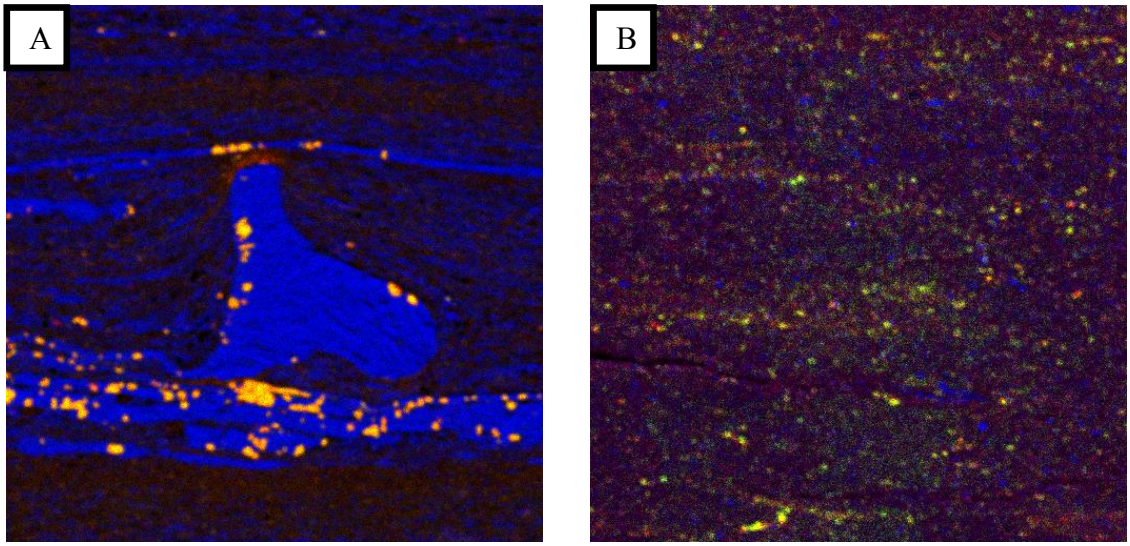

Figure 21: X-ray images of samples from zone 3 in the Maness Shale. Composite images were created by stacking and applying color identifiers to Ca (blue), Fe (red), and S (green). The yellow color shows pyrite grains. (A) is from well A at a depth of 8,140' and (B) is from well B at a depth of 9,150'.

3.2.2 Zone 4

Zone 4 has some of the highest TOC and redox-sensitive trace element concentrations within the eight zones. X-ray images show a mostly laminated lithofacies within this zone (Figure 22). The laminations show variation in the amount and composition of sediments deposited during this time. The presence of continuous, well preserved laminations indicates few to no burrowing organisms were present during

deposition which suggests low oxygen levels. Pyrite laminations are well defined and grade up into more carbonate rich layers that are less defined (Figure 20 B). A more massive mudstone micro-facies lies above the laminated micro-facies as a result of increased bioturbation indicating more oxygenated conditions. In the more massive micro-facies, Fe is primarily in elemental form with more minor amounts present in disseminated pyrite.

Sample B shows high levels of Ca (15.6%) with relatively lower levels of Fe (2.0%) and S (0.8%) as measured by whole-rock elemental analysis. Mo is relatively low at 31 ppm while V is high measuring 890.7 ppm. TOC is very high in sample B measuring 6.32 wt. %.

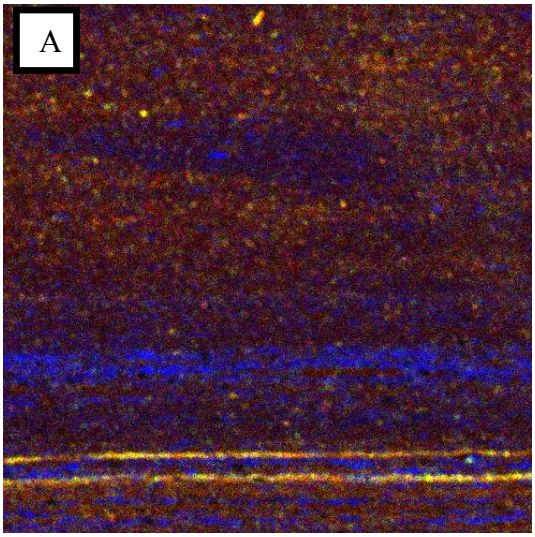

Figure 22: X-ray images of sample from zone 4 in the Maness Shale. Lamination colors are the result of different elements stacked on top of each other. When lamination is blue, there is more Ca present. (A) is from well B at a depth of 9,160'. Color scheme is the same as in Figure 19.

3.2.3 Zone 5

Zone 5 also has some of the highest TOC and redox-sensitive trace element concentrations measured in the 8 zones. X-ray images show an abundance of pyrite in zone 5 as seen in Figure 23. Pyrite is seen in a fine, continuous form in sample A and in more massive, clotted bands in sample B. Sample A in Figure 23 contains high levels of Ca (15.2%), Fe (4.1%), and S (2.0%) as measured from whole-rock elemental analysis. This is in association with high concentrations of Mo (139.8 ppm) and V (1215.7 ppm). Sample B shows similar element concentrations with high levels of Ca (29.7%), Fe (4.27%), and S (1.9%). Mo and V concentrations are not as high as what is seen in sample A measuring 15.1 ppm and 358.8 ppm respectively.

Sample B from well B shows an abundance of Ca (shown in blue) throughout the matrix intermixed with organic material (shown in black). This appears to be the same diagenetic calcite as what was shown previously in thin sections from well B in Figure 15. Organic material can also be seen in association with pyrite in sample be shown as black spots within the yellow pyrite. TOC is highest in sample A (5.8 wt. %) and 3.8 wt. % near sample B. TOC may be reduced in sample B due to calcite dilution.

3.3 Chemostratigraphic Zones within a Sequence Stratigraphic Framework

The stratigraphy of the Woodbine/Maness interval is closely tied with the tectonic history of the Gulf Coast as well as with eustatic changes in sea level (Adams and Carr, 2010). The Maness Shale is a net transgressive package which unconformably overlies the Buda Limestone and unconformably underlies the Woodbine clastics and is a member of the Washita Group which is lower Cenomanian in age.

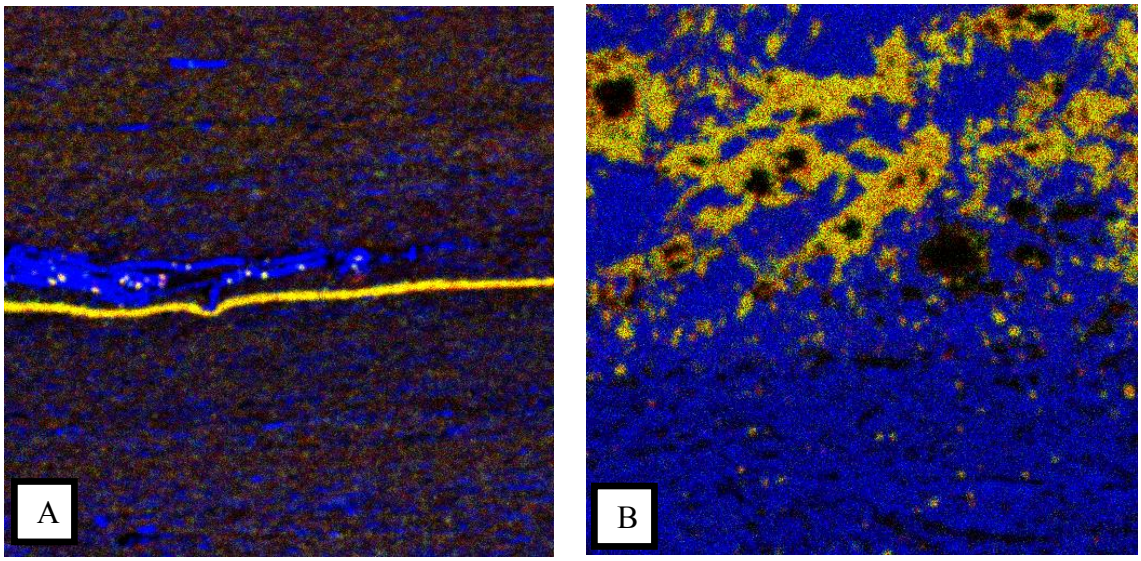

Figure 23: X-ray images of samples from zone 5 in the Maness Shale. (A) is from well A at a depth of 8,152' and (B) is from well B at a depth of 9,175'. Color scheme is the same as in Figure 19.

The lower half of the Maness Shale is a thick retrogradational package present throughout the East Texas Basin which averages ~50' in the study area and represents a third-order transgressive systems tract with an associated maximum flooding surface (MFS) dated at approximately 93.5 Ma (Ambrose et al., 2009). There is a condensed

section associated with the MFS which contains dark organic and carbonate rich mudstones near the middle portion of the Maness interval.

The Woodbine Group is composed of Woodbine clastics and their distal equivalent the Pepper Shale. It unconformably overlies the Maness Shale and is a third-order regressive-transgressive sequence with minor smaller sequences locally present (Adams and Carr, 2010). The Woodbine clastics are located within the East Texas Basin and are primarily deltaic facies containing meanderbelt fluvial, shelf strand plain, and high-destructive depositional systems (Ambrose et al., 2008). The Pepper Shale is composed of prodelta mudstones deposited onto the outer shelf and slope of the East Texas Basin. The Pepper/Woodbine Group are age equivalent to the Lower Eagle Ford of South Texas according to biostratigraphic data derived from nanofossils and foraminifera assemblages present within the section.Volcanic sediments are rare in the Woodbine sediments in east Texas but are common in the Eagle Ford/Sub-clarcksville interval.

The Eagle Ford/Sub-clarksville sequence unoconfromably underlies the Austin Chalk and unconformably overlies the Woodbine Group. Most of the section is erroded at the top by the major “Eagle Ford Unconformity” which is described as a critical lowstand event by Adams and Carr (2010) and is present across much of the Gulf Coast. Locally the Eagle Ford/Sub-clarksville sediments are preserved within incised valleys. These sediments are composed of limestone facices which contain foraminifera and pelecypod fragments intermixed with non-marine to shallow marine clastic sediments.

Biostratigraphic data ties the age of the Eagle Ford/Sub-clarkville section to the Upper Eagle Ford of South Texas.

Figure 24 shows the chemozonations within the interpreted sequence stratigraphic framework along with a plot of measured TOC. Zones 6, 7, and 8 are within packages of stacked parasequences unconformably overlying the Buda Limestone and bounded by marine flooding surfaces in the net transgressive lower Maness. Zones 3, 4, and 5 are within the condensed section associated with a maximum flooding surface at the top of zone 3. Zone 2 is within a regressive package in the upper Maness which is bounded on top by a sequence boundary. Zone 1 is within the transgressive to regressive Pepper Shale which is bounded at the top by a sequence boundary and overlain by the Austin Chalk.

Sequences within the Maness and Pepper Shale correlate with TOC and other organic chemical data. The Maness and Pepper Shale interval were deposited within a constructional shelf margin in which significant organic rich rocks accumulate (Passey et al., 2010). In this setting, TOC generally increases within each parasequence toward a flooding surface. This vertical stacking pattern can be seen in zones 7, 6, 2, and within some sequences in zone 1. Chemo zones 8 and some sequences in zone 1 show an opposite trend where TOC decreases upwards. It has been noted by Creany and Passey (1993) that within discrete sedimentary units within organic-rich shales, TOC values are often observed to be highest at the base decreasing toward the top of the unit. This vertical profile can be explained by an increase in sedimentation rate as sediments begin

to fill the basin and dilute TOC (Creany and Passey, 1993). These sequences may be depositied as part of a late hightand to early transgressive systems tract where sedimentation rates begin to steadily increase. There may also be a change in organic matter type in which more terrigenous, lower hydrogen organic matter is being deposited and thus lower TOC.

Another common stacking pattern observed by Creany and Passey (1993) in which TOC increases from the base to a central TOC maximum then decreases toward the top of the unit. This stacking pattern is seen within the condensed section of both wells where TOC reaches it's maximum at the contact between zones 4 and 5. Creany and Passey note that under primarily anoxic conditions, accomidation space becomes the main controlling factor in in the formation of organic-rich rocks. Redox-sensitive elements indicate that the environment was anoxic to euxinic so the increase in TOC toward the contact between zones 4 and 5 must be driven by an increase in water depth and relative accomodation which lead to low sedimentation rates and low dilution of organic material. As sea level reached it's maximum and began to fall, a decrease in accomidation space caused an increased rate of sedimentation and possibly increased levels of oxygen into the basin as indicated by a drop in redox-sensitive elements in zone 3 where TOC is lowest in the condensed section.

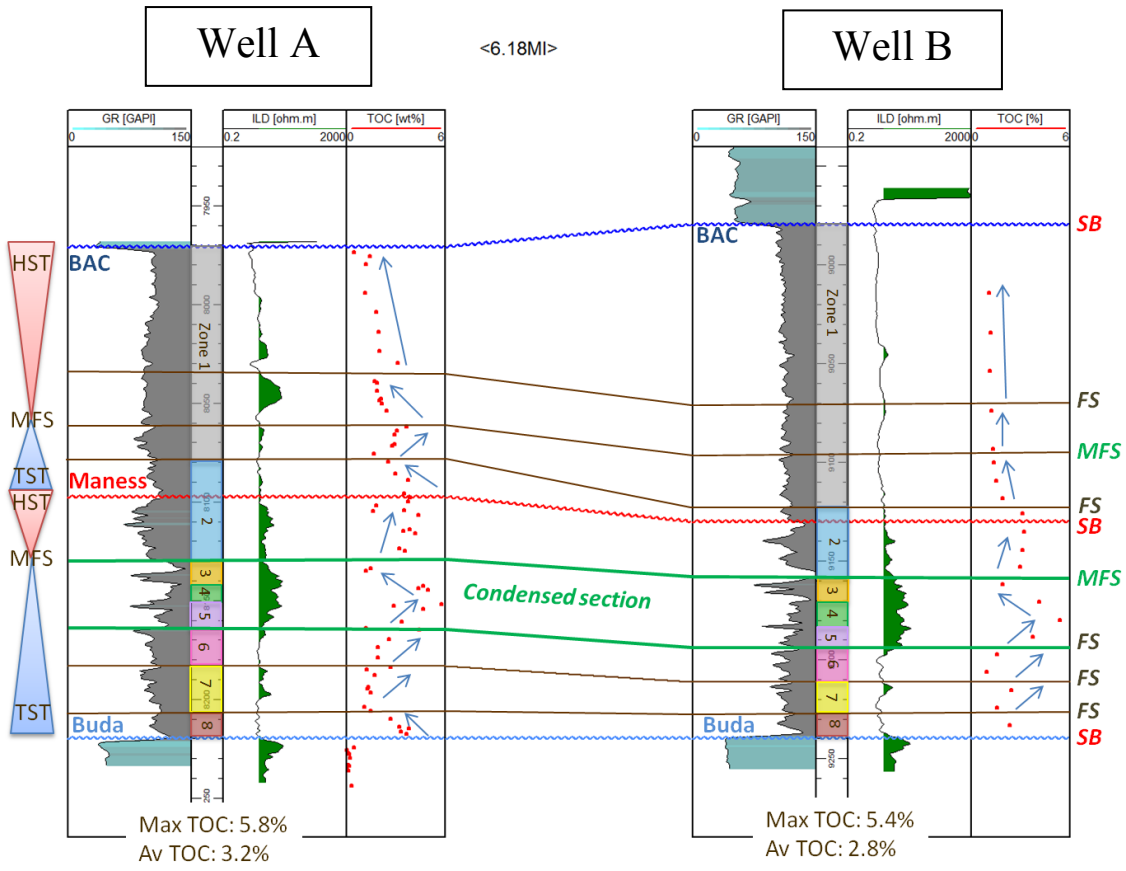

Figure 24: Sequence stratigraphy of the Maness/Woodbine interval. Chemo zones are labeled in the depth track within the well logs. SB = sequence boundary, FS = flooding surface, MFS = maximum flooding surface.

Similar vertical distribution trends can be seen with the Hydrogen Index (HI) (figure 25). Increases and decreases in HI closely mirror those observed in TOC. This is best documented in well A which is lower maturity (Ro = 0.9) than in well B (Ro = 1.2). As kerogen matures and converts to hydrocarbons, hydrogen becomes depleted and therefore HI levels become lower than their original levels (Jarvie, 2012). Because well A is more mature, most of the original HI has been depleted and thereofore HI measurements are low.

HI and TOC are inherently related as increasing TOC is due to increased algal content which contains high levels of hydrogen (Passey et al., 2010). There would be an inverse relationship if the nature of the kerogen was more woody and coaly which has low HI. Visual kerogen analysis as well as data from programmed pyrolyis indicate that the kerogen types found in the Maness Shale are predomiantly TypeII/III which is more rich in hyrdrogen and explains the correlative nature of TOC and HI.

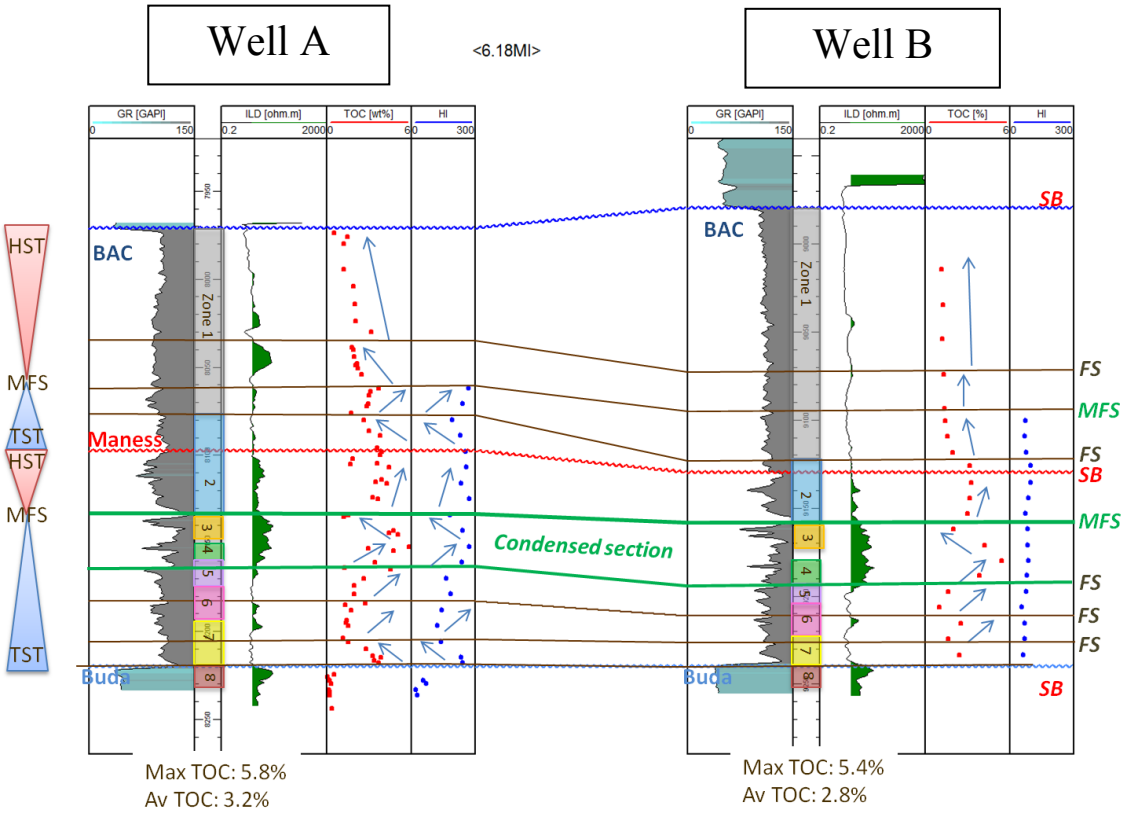

Figure 25: Comparison of TOC to HI vertical stacking distribution within interpreted sequence stratigraphic framework.

3.4 Source Rock Analyzer/TOC/VRo Analysis

Total organic carbon (TOC) measures the organic richness of sedimentary rocks (Jarvie, 1991). It is one of the most commonly used screening analyses for determining the organic richness of a sediment sample (Jarvie, 2012). TOC greater than 1% is needed to determine the presence of a viable source rock (Liro et al., 1994). Core samples for well A and B have been collected for source rock evaluation. Leco derived TOC was used to determine organic content for each well. For well A, the average TOC for the Pepper Shale is 3.3% ranging from 2.3% to 3.9% and 3.2% with a range of 1.5% to 5.8 for the Maness Shale (Table 2). For well B, the average TOC for the Pepper Shale is 1.7% ranging from 1.1% to 3.1% and 2.8% ranging from 1.0% to 5.4% in the Maness Shale (Table 3). The measured TOC values are within the range of a good source rock.

Whether a source rock will generate oil or gas is dependent upon the source of the organic matter and its degree of preservation (Liro et al., 1994). Oil prone material is hydrogen rich and displays elevated hydrogen index (HI) values greater than 400 (Liro et al., 1994). HI averages 221 mg/g HC ranging from 162-269 mg/g HC within the Pepper Shale in well A and 210 mg/g HC ranging from 140 to 275 mg/g HC in the Maness Shale (Table 2).

Top Depth (ft)	Sample Prep	Sample Type	Leco TOC	S1	S2	S3	Tmax (°C)	Calc. %Ro	Meas. %Ro	HI	OI
8062		core chips	3.68	5.05	9.91	0.29	446	0.87		269	8
8062	extracted	core chips	3.45	2.08	8.33	0.24	454	1.01		241	7
8071		core chips	2.96	3.14	7.13	0.30	445	0.85		241	10
8080		core chips	2.60	3.10	5.00	0.25	446	0.87		192	10
8080	extracted	core chips	2.26	0.08	4.01	0.10	453	0.99		177	4
8089		core chips	3.79	2.98	8.76	0.28	446	0.87		231	7
8098		core chips	3.90	3.44	10.04	0.30	445	0.85		257	8
8098	extracted	core chips	3.50	0.13	5.66	0.12	452	0.98		162	3
8107		core chips	4.40	4.70	11.47	0.35	446	0.87		261	8
8116		core chips	4.25	3.31	9.97	0.37	445	0.85		235	9
8116	extracted	core chips	3.92	3.50	9.39	0.41	453	0.99		240	10
8125		core chips	3.69	5.62	10.04	0.35	446	0.87		272	9
8134		core chips	1.48	2.81	2.69	0.32	445	0.85		182	22
8134	extracted	core chips	2.23	3.06	3.32	0.24	451	0.96		149	11
8143		core chips	4.72	4.97	11.42	0.39	443	0.81		242	8
8152		core chips	5.83	3.66	16.02	0.34	446	0.87		275	6
8152	extracted	core chips	5.23	4.31	13.54	0.48	446	0.87		259	9
8161		core chips	3.42	2.98	8.11	0.32	443	0.81		237	9
8170		core chips	2.64	1.92	4.32	0.26	441	0.78		164	10
8170	extracted	core chips	2.46	1.84	5.50	0.26	453	0.99		224	11
8179		core chips	1.93	1.62	3.59	0.28	443	0.81		186	15
8188		core chips	1.74	0.70	2.48	0.20	446	0.87		143	11
8188	extracted	core chips	1.65	0.68	2.31	0.17	455	1.03		140	10
8197		core chips	1.51	0.65	1.87	0.17	445	0.85		124	11
8206		core chips	1.50	1.13	2.11	0.25	441	0.78		141	17
8206	extracted	core chips	1.99	1.17	3.28	0.23	454	1.01		165	12
8215		core chips	3.84	2.55	9.06	0.29	448	0.90		236	8
8218.1		core chips	3.91	2.80	9.94	0.33	446	0.87		254	8
8218.1	extracted	core chips	3.61	2.38	8.74	0.35	452	0.98		242	10
8218.1		core chips	3.68	2.78	8.91	0.34	447	0.89		242	9
8228		core chips	0.21	0.06	0.12	0.18	390	-1.00		57	86
8230		core chips	0.28	0.08	0.19	0.18	362	-1.00		68	64
8233.5		core chips	0.14	0.01	0.03	0.19	381	-1.00		21	136
8236.5		core chips	0.17	0.01	0.05	0.15	320	-1.00		29	88

Table 2: Leco TOC and Rock-Eval data from well A core.

HI averages 80 mg/g HC ranging from 71 to 99 mg/g HC in the Pepper Shale in well B and 77 mg/g HC ranging from 57 to 97 mg/g HC in well B (Table 3). HI for both wells are below the 400 mg/g HC threshold for good generative capability however these values are reduced from what they were when they were immature before they began generating and expelling hydrocarbons (Edman and Pitman, 2010).

Top Depth (ft)	Sample Prep	Sample Type	Leco TOC	S1	S2	S3	Tmax (°C)	Calc. %Ro	Meas. %Ro	HI	OI
9000	extracted	core	1.13								
9020	extracted	core	1.23								
9040	extracted	core	1.20								
9060	extracted	core	1.30								
9080	extracted	core	1.35								
9087	extracted	core	1.42	0.12	1.04	0.10	468	1.26		73	7
9096	extracted	core	1.56	0.11	1.11	0.08	467	1.25		71	5
9100	extracted	core	2.29								
9105	extracted	core	1.95	0.33	1.53	0.08	464	1.19		78	4
9114	extracted	core	3.15	0.49	3.12	0.07	473	1.35		99	2
9123	extracted	core	3.26	0.27	3.17	0.10	468	1.26		97	3
9132	extracted	core	3.14	0.64	2.74	0.12	464	1.19		87	4
9141	extracted	core	3.00	0.55	2.22	0.10	467	1.25		74	3
9150	extracted	core	1.97	0.44	1.64	0.08	468	1.26		83	4
9159	extracted	core	4.19	0.16	3.58	0.09	468	1.26		85	2
9168	extracted	core	5.43	0.15	4.68	0.10	468	1.26		86	2
9177	extracted	core	3.81	0.20	3.00	0.10	467	1.25		79	3
9186	extracted	core	1.60	0.17	1.24	0.06	466	1.23		77	4
9195	extracted	core	0.98	0.19	0.56	0.00	455	1.03		57	0
9204	extracted	core	2.51	0.25	1.78	0.06	467	1.25		71	2
9213	extracted	core	1.62	0.32	1.11	0.03	461	1.14		69	2
9222	extracted	core	2.39	0.27	1.45	0.04	469	1.28		61	2

Table 3: Leco TOC and Rock-Eval data from well B core.

Kerogen is classified into three types: Type I, Type II, and Type III as determined by a van Krevelen diagram. A van Krevelen diagram is a graph of hydrogen index (HI) vs. oxygen index (OI) plotting OI on the Y axis and hydrogen index HI on the X axis. The type of kerogen depends mainly on the value of the HI.

Type I kerogen is mostly of lacustrine origin and has original HI values greater than 700 mg HC/ g TOC according to the van Krevelen diagram in figures 26 and 27. Type II kerogen is of marine origin and has original HI values ranging from 350 to 700 mg HC/ g TOC. Type III is mostly woody material of terrestrial origin and has original HI values less than 175 mg HC/ g TOC.

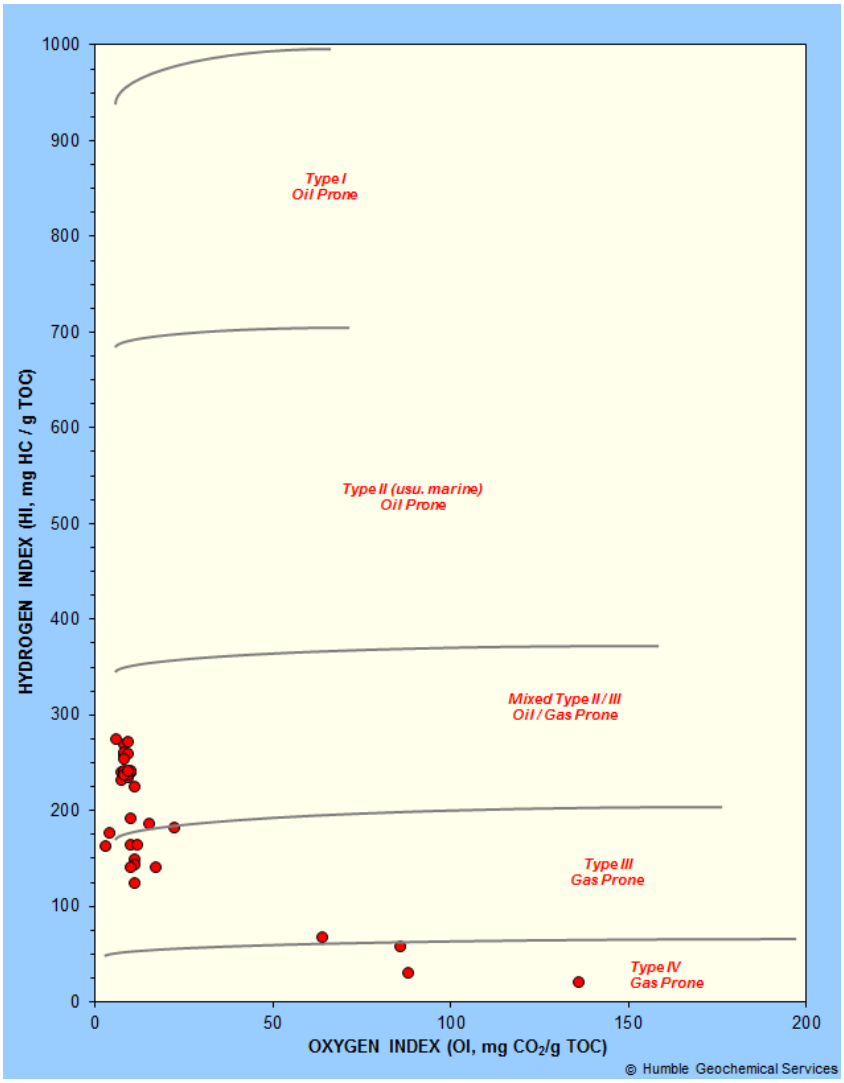

Figure 26: Van Krevelen diagram for well A showing a mixture of Type II/III and Type III kerogen.

The Maness and Pepper Shale samples taken from the two cores indicate there is primarily a mix of Type II/III and Type III kerogen. Type II kerogen is derived from marine plankton and generates more oil than Type III which is derived from terrestrial higher plants which will produce more gas (Langford and Blanc-Valleron, 1990).

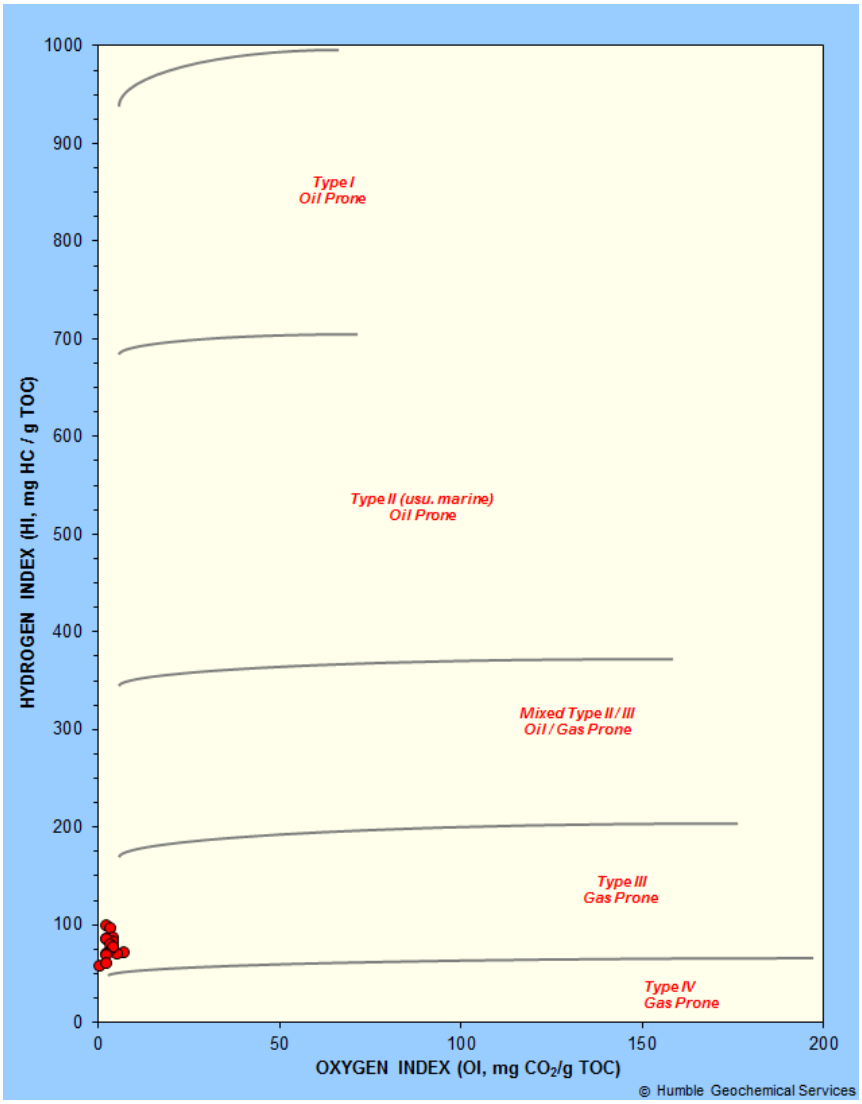

Figure 27: Van Krevelen diagram for well B showing Type III kerogen.

Type II kerogen is often deposited in transgressive systems with increased OM enrichment and generation potential while woody, gas prone Type III kerogen is more suggestive of regressive conditions (Liro et al., 1994). It is likely that when these samples were immature that they were a Type II kerogen which is common for marine

settings which are indicated for the Maness and Pepper Shales (Edman and Pitman, 2010).

Three core samples between 9,086.9’ to 9,185.75’ from well B have been analyzed using visual kerogen analysis to determine maturation (VR-vitrinite reflectance or Ro and TAI-thermal alteration index) to verify the Rock-Eval HI and Tmax data. The measured Ro values vary from 1.25% to 1.28%. There was good organic recovery in all 3 samples; however, there were not the desired 40 vitrinite particles in 2 of the 3 samples. The Rock-Eval Tmax values for well B range from 455 to 473°C which is equivalent to an Ro of 1.2 to 1.4%. This is in good agreement with the measured Ro values.

3.5 Element Comparisons to TOC

Redox-sensitive trace metal measurements were plotted against TOC to determine their relationship to the amount of organic carbon present within each chemo zone. The highest measured TOC is found within the condensed section which is comprised of zones 3, 4, and 5 with average TOC values of 3.21 and 4.27 wt. % for well A and B respectively. These zones also show the highest levels of redox-sensitive trace elements Cu, Ni, V, Mo, and U as shown in figures 28 and 29. The lowest TOC is seen in zones 6 and 7 in the lower Maness Shale averaging 1.92 and 2.07 wt. % for well A and B respectively. Correspondingly, these zones have the lowest levels of redox-sensitive trace elements.

Cu and Ni show the best ties to TOC, especially in well B with an R^2 of 0.94 and 0.88 respectively. Figures 30 and 31 shows cross plots of Cu vs. TOC and Ni vs. TOC; a positive correlation is seen in well B with these elements increasing with increasing TOC. This same trend for Cu and Ni is not as clear in well A with R^2 values of 0.33 and 0.30 respectively. Plots of Cu vs. TOC were broken out by groupings of chemo zones for each well, however, no coincident points for Cu and Ni with TOC in zones 6-8 were present in well B, only well A.

Zones 1-5 show the best correlation while zones 6-8 in the lower Maness Shale do not show a positive correlation to TOC. Figure 30 shows 2 plots with Cu and TOC for well A; one with just zones 1-5 and the other with all zones. Zones 1-5 have an R^2 of 0.5 indicating a good relationship between Cu and TOC. Zones 6-8 have and R^2 value of

0.33 indicating a poor relationship between Cu and TOC. This may indicate that the deposition and preservation of organic material is not tied to the redox levels in the water column or by the productivity levels of marine organisms since Cu acts as a micronutrient and therefore is an indicator of marine productivity. This may also be the case for well A which contains high levels of TOC but no clear trend with Cu and Ni is seen.

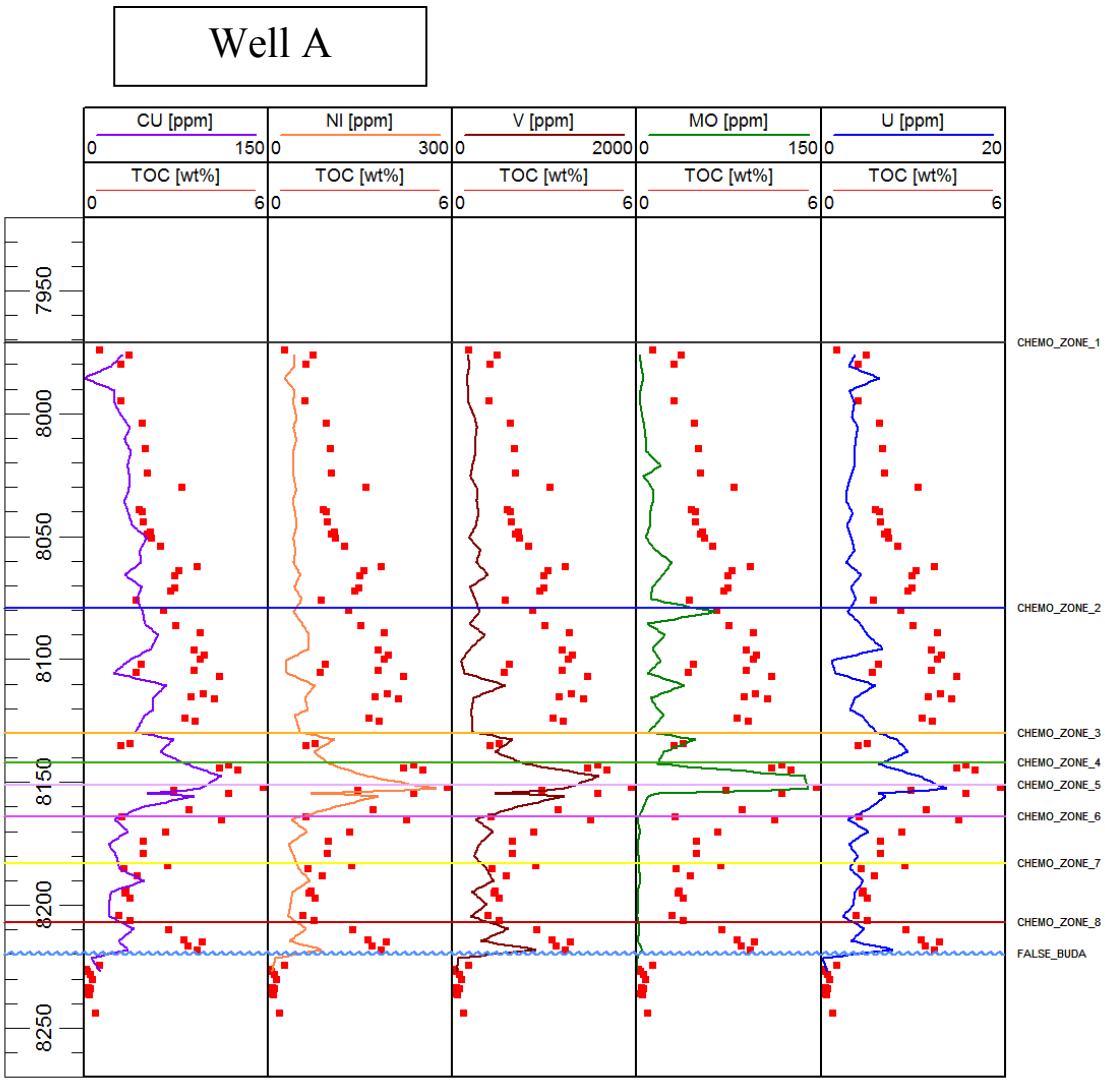

Figure 28: Comparison of redox-sensitive trace metals to TOC.

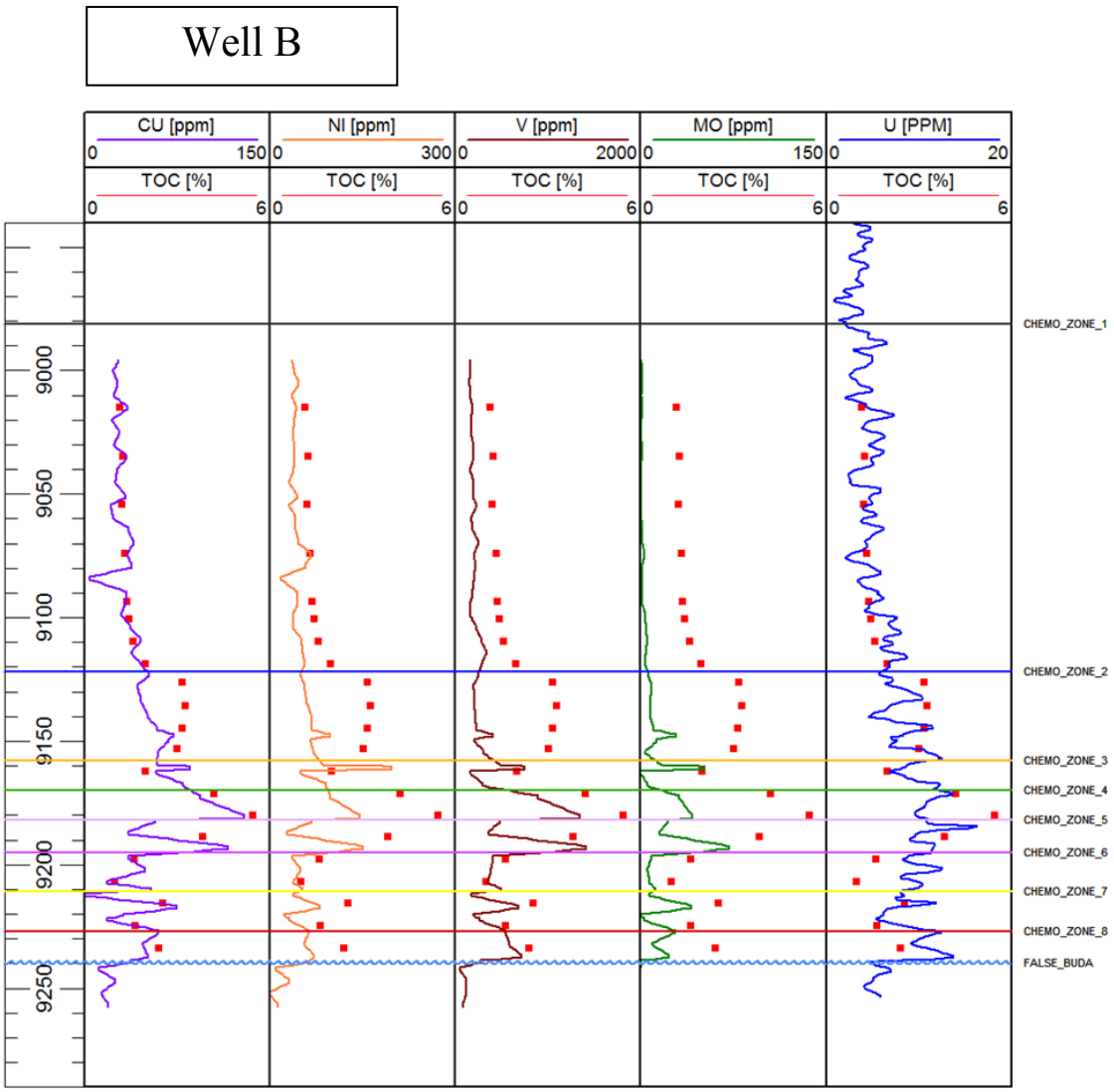

Figure 29: Comparison of redox-sensitive trace metals to TOC.

Ni has a very good correlation with TOC in well B with an R^2 value of 0.88 similar to what was seen with Cu (Figure 31). Well A shows a very poor relationship with an R2 value of 0.30 for all zones. There is however one data point at a depth of 8,152' from zone 5 that shows a very strong correlation between Ni and TOC. Other redox-sensitive elements such as Mo and V (Figure 28) are also very high at this depth

suggestive of an anoxic to euxinic environment of deposition which preserved organic matter.

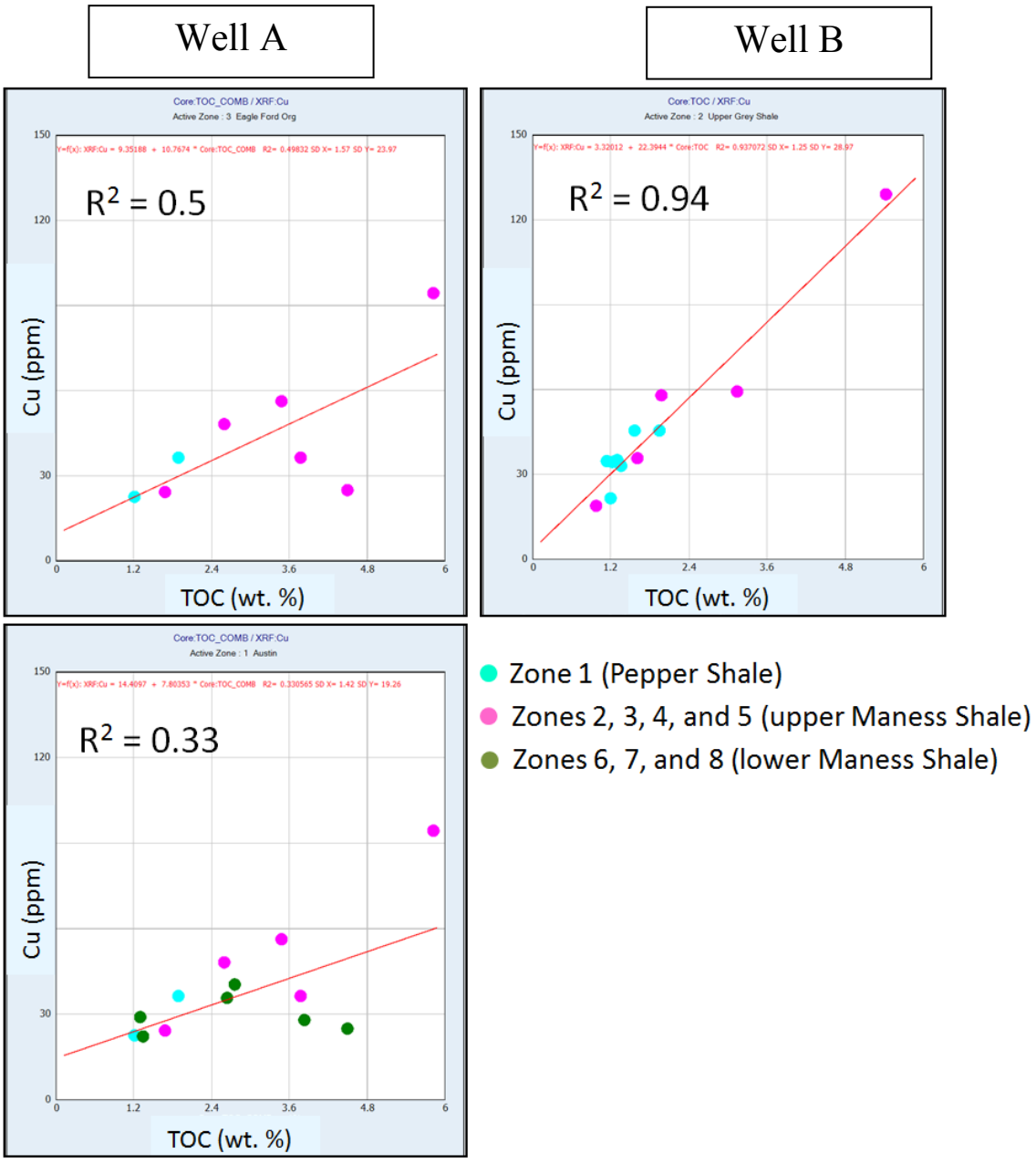

Figure 30: Cu and Ni vs. TOC for wells A and B.

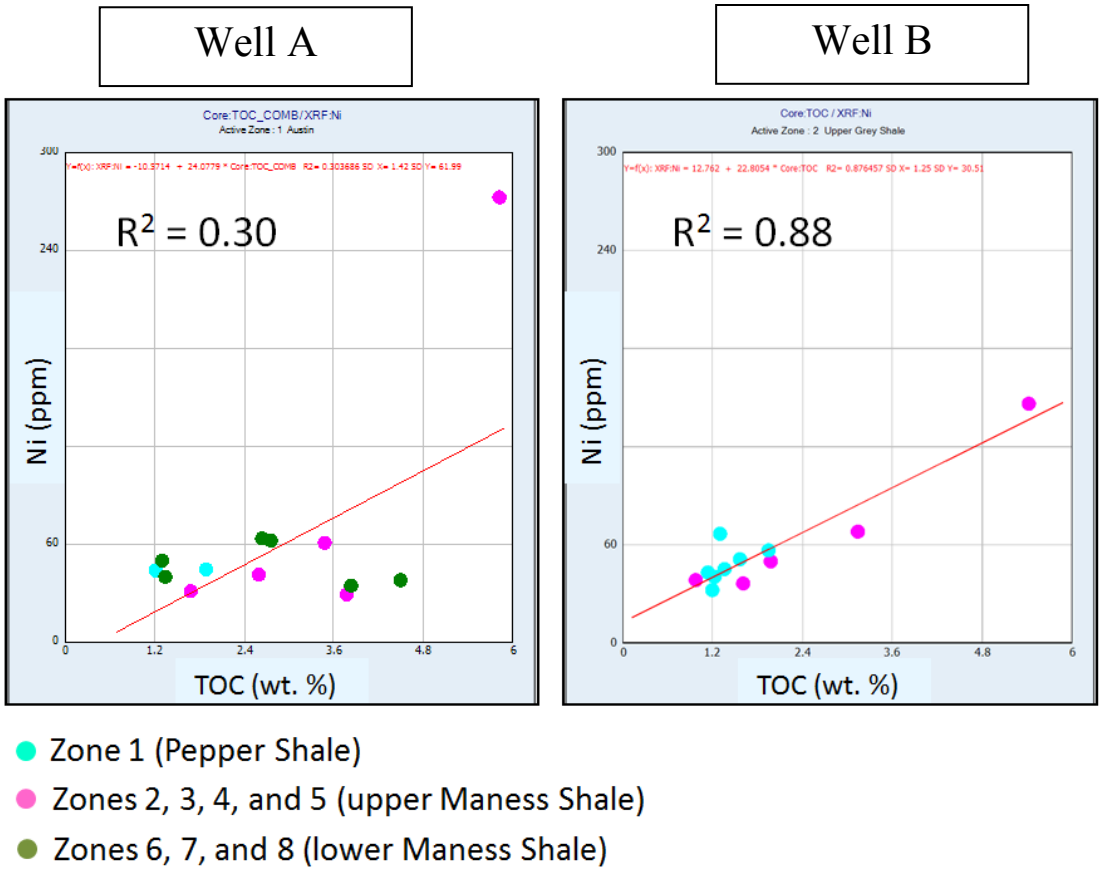

Figure 31: Ni vs. TOC for wells A and B.

Good correlations are seen between V, Mo, and U with TOC in well B (Figure 32). These elements are good indicators of paleo-redox conditions and indicate that conditions for well B were anoxic to euxinic in some zones, primarily in zones within the upper Maness Shale shown in the cross plots as pink. Based on this relationship, it can be inferred that anoxic conditions, which may be a result of increased microbial productivity, lead to the preservation of organic material within well B.

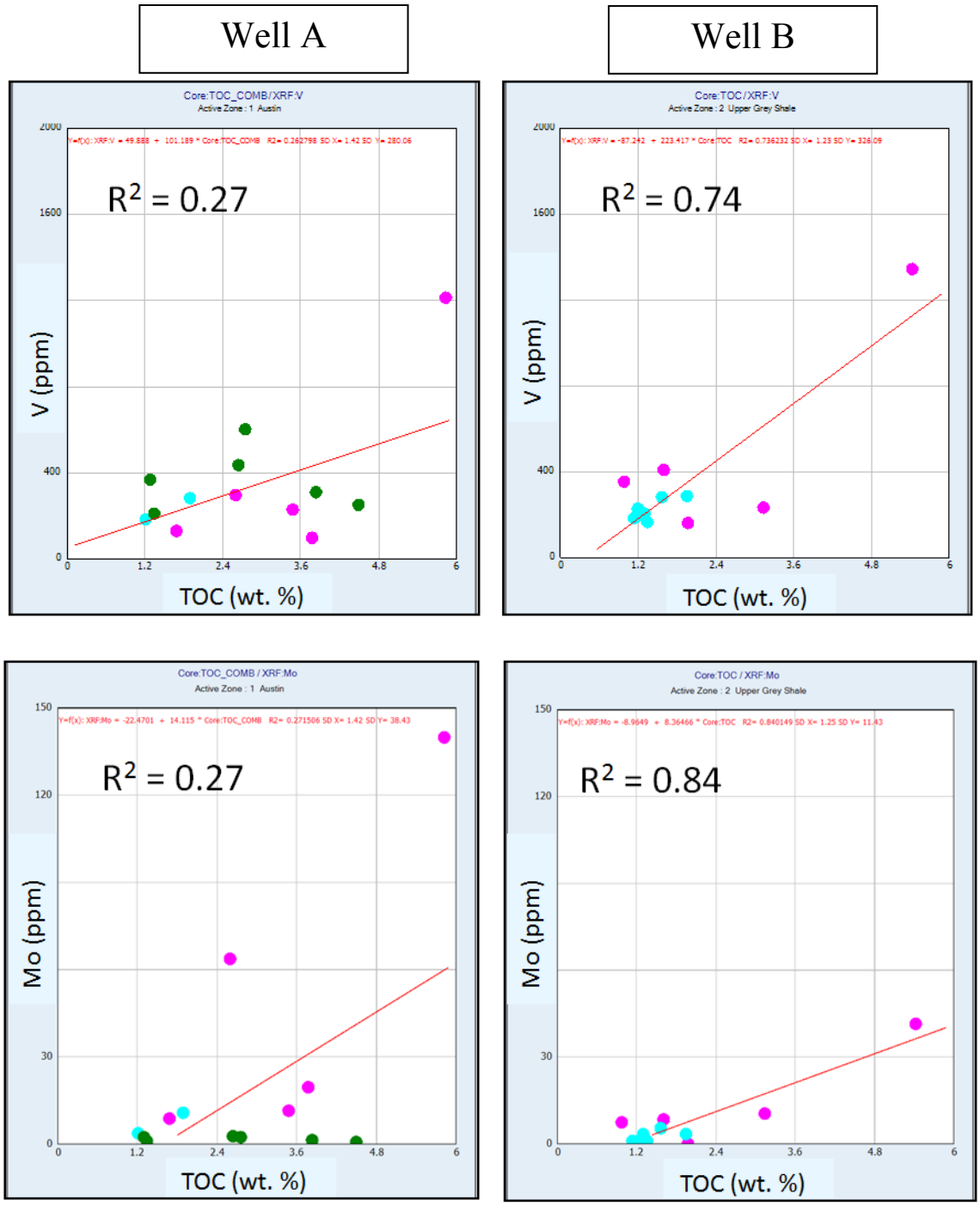

Figure 32: V, Mo, and U vs. TOC in wells A and B.

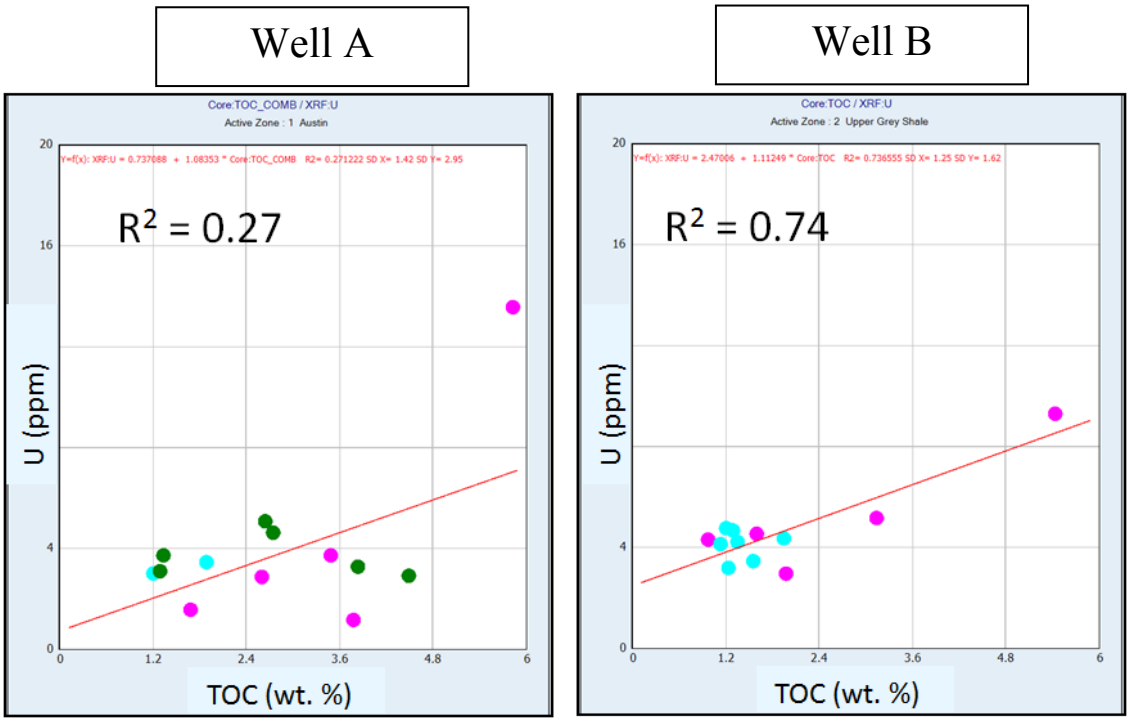

Figure 32 (*Continued*)

This does not appear to be the case for well A which shows a poor relationship between V, Mo, and U with TOC. Zones in the upper Maness are enriched in these elements indicating overall reducing conditions, however there may be another more dominant mechanism that controls organic matter deposition and preservation in well A. As was seen in the Cu and Ni plots, there is an outlier point from zone 5 which shows very high levels of these elements in connection with high TOC; this data point shows very high concentrations of Mo (140 ppm) indicating this sample was deposited under oxygen-depleted, euxinic conditions where free H_2S was present in the water column. Because this data point has high TOC (5.23 wt. %) it can be inferred that euxinic conditions lead to the preservation of organic material within the sediment column.

3.6 Relationship of Carbonate Content to TOC

A strong correlation is seen between Ca and TOC in well B with an R^2 of 0.80 (Figures 33 and 34). This however is not the case for well A which shows an R^2 value of 0. This follows the same trends seen earlier with other elements plotted against TOC in well A.

For well B, the positive correlation in Ca vs. TOC and Cu vs. TOC, particularly seen in zones 3, 4, and 5, indicate that TOC is controlled by high levels of authigenic marine productivity since Cu acts as a productivity indicator. The increase in Ca is related to biogenic carbonate material, mostly calcite, from foraminifera tests and other skeletal debris. There is an outlier data point at a depth of 9,150' in well B which contains a high percentage of Ca (12%) with lower TOC (1.97 wt. %). This data point is from zone 3 which is located near the MFS at the top of the condensed section in the Maness Shale. Thin sections from this zone show an abundance of foraminifera and inoceramid fragments; this increase in calcite can be seen in wire line logs as a low GR spike which is correlatable around the study area. The high concentration of calcium related to biogenic skeletal debris implies that the organic content in this zone has been diluted by the abundance of carbonate material.

Well A does not show any correlation between Ca and TOC indicating there is a different relationship than what is observed in well B. Figure 29 shows that zones 4 and 5 in well A contain high levels of TOC while the Ca curve measured from XRF is low. FTIR mineralogy measurements show that well A contains lower total carbonate content

(45.0%) than well B which contains 51.6% within the condensed section (zones 3, 4, and 5). Since well A has lower Ca content and did not show a good correlation between Cu and TOC, it can be inferred that something other than authigenic marine productivity is controlling the deposition and preservation of organic material.

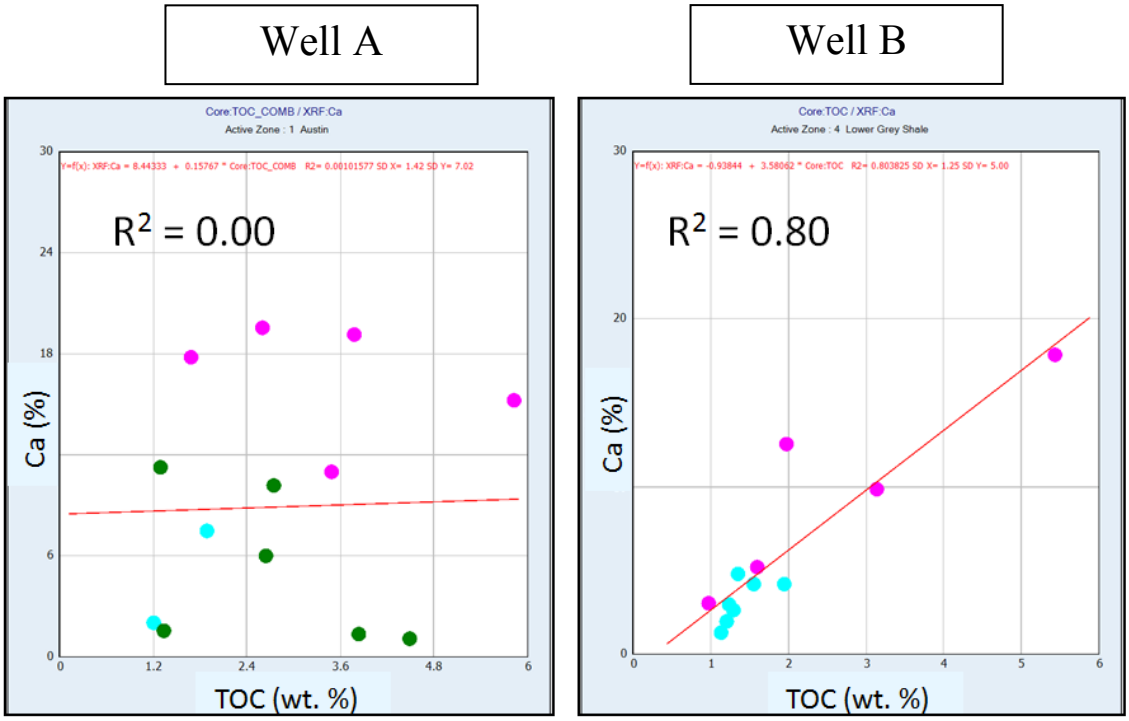

Figure 33: Ca vs. TOC for wells A and B.

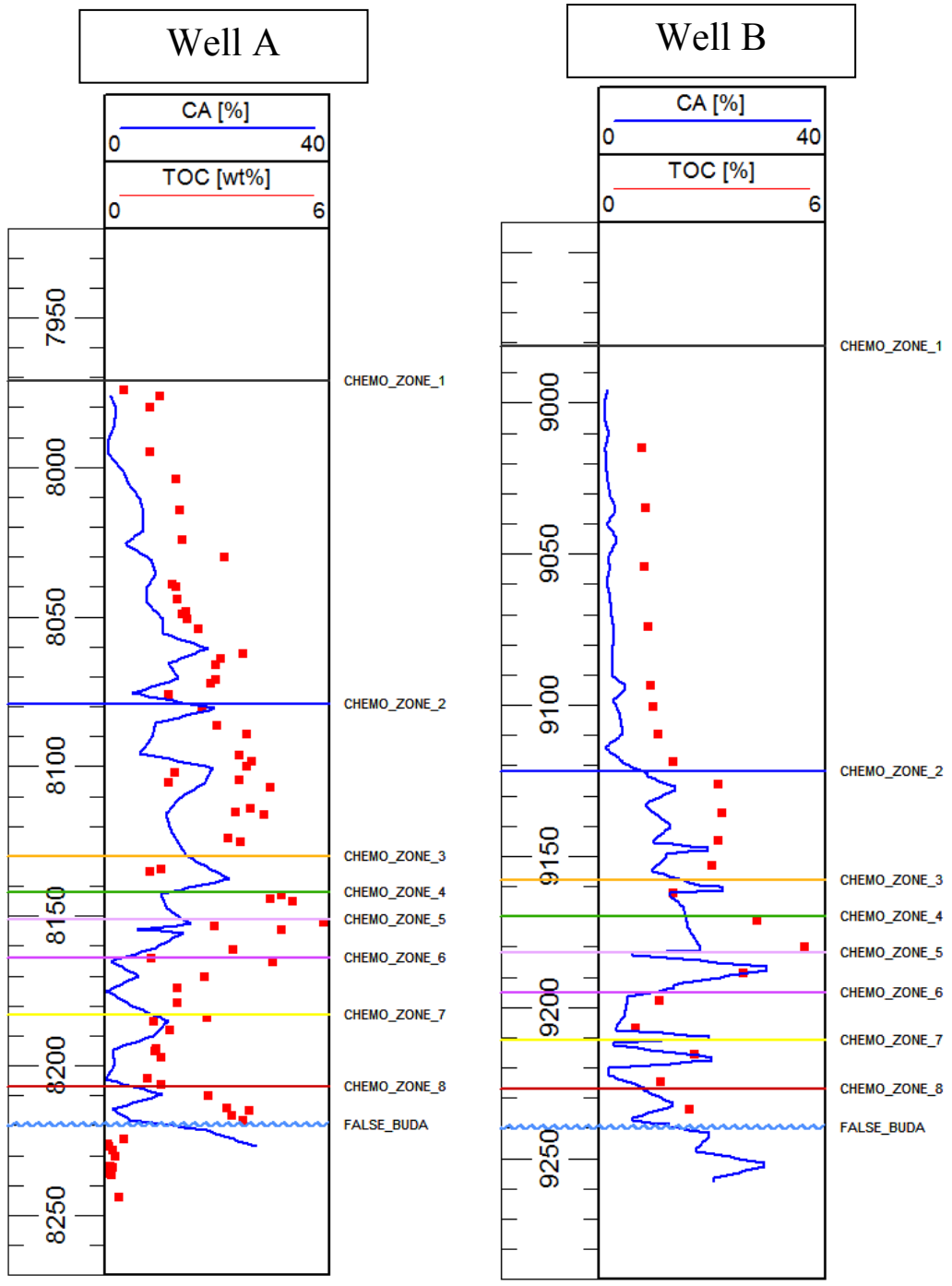

Figure 34: Vertical profile of the relationship between Ca and TOC in wells A and B.

3.7 Depositional Controls on Source Rock Development

To understand the depositional controls on organic matter deposition and preservation, two different depositional models are proposed based on the source of organic material and method of preservation. One is based on deposition mainly from terrestrially sourced sediments and organic material while the other is based on more authigenic deposition from within the water column from biologic activity. In the first model, organic preservation is driven by sediment deposition rates and clay content while the latter is driven by anoxia.

As was shown earlier in Figures 30 and 31, zones 6, 7, and 8 in the lower Maness Shale do not show a positive correlation between Cu and Ni vs. TOC which averages 2.2 wt. % (Table 4). This means that TOC within these zones is not sourced from marine productivity but rather by more terrigenous organic material being brought into the basin. Detrital indicators Al, Ti, and Th show an increase through these zones which also indicate more terrigenous input. Clay content is high as shown in Table 5 measuring 54.7% in well A and 60.8% in well B. Redox-sensitive elements are lower in these zones (Table 6) indicating preservation may be a combination of anoxia and clay content/sediment burial rates.

Zones 3, 4, and 5 do show a positive correlation between Cu and Ni vs. TOC which averages 3.7%. This indicates that organic material in these zones was sourced from marine productivity. The correlation is strongest in well B which is further downdip in a more distal location relative to the paleo-shoreline. Detrital indicators Al,

Ti, and Th are low through these zones which means there are little terrigenous sourced sediments. Average clay content is lower than what was measured in the previous zones averaging ~37% in each well. Redox-sensitive elements are the highest in these zones indicating maximum basin restriction during this time and organic preservation by anoxia.

Zone 2 shows similar trends to what is seen in the previous zones (3, 4, and 5) but does show an increase in clay content (~43%) with a decrease in redox-sensitive elements. TOC averages 3.3 wt. % similarly to what is measured in zones 3, 4, and 5. This zone shares a similar depositional style to zones 3, 4, and 5 but with higher terrigenous input and a mix of preservation methods.

Well Name and Zones	Quartz	Calcite	Dolomite	Siderite	Total Clays	Total Feldspars	Pyrite	No. of Measurements
Well A								
Zone 1 (Pepper Shale)	2.67	14.35	1.35	7.19	63.48	7.29	1.54	63
Zone 2 (top Maness Shale)	2.62	31.66	3.86	8.07	42.59	6.24	0.90	29
Zones 3, 4, and 5 (Condensed Section)	1.10	34.76	4.33	5.90	37.81	13.00	0.33	21
Zones 6, 7, and 8 (Lower Maness)	5.39	12.45	2.68	6.94	54.65	14.87	0.65	31
Totals	2.95	23.31	3.06	7.03	49.63	10.35	0.86	180
Well B								
Zone 1 (Pepper Shale)	2.65	6.67	1.05	6.95	72.80	6.05	1.33	73
Zone 2 (top Maness)	1.00	27.88	5.41	10.18	44.94	6.24	0.82	17
Zones 3, 4, and 5 (Condensed Section)	0.57	40.67	1.81	9.10	37.19	5.05	0.95	21
Zones 6, 7, and 8 (Lower Maness)	2.42	13.88	2.35	8.15	60.81	7.27	1.54	26
Totals	1.66	22.28	2.66	8.60	53.94	6.15	1.16	137

Table 4: Average mineral compositions for chemo zones based on FTIR measurements from wells A and B.

Zone 1 somewhat shows a positive correlation between Cu and Ni vs. TOC however, TOC levels are lowest in this zone on average (1.8 wt. %) and concentrations of Cu and Ni are at the lowest levels seen in any of the zones. Clay content is very high averaging 63.5% in well A and 72.8% in well B. Detrital indicator elements Al, Ti, and Th are all very high indicating high levels of terrigenous input at the time of deposition. Organic material may have been more terrestrially sourced and preservation was poor due to oxic conditions.

Well Name and Zones	Cu (ppm)	Ni (ppm)	V (ppm)	Mo (ppm)	U (ppm)	Th (ppm)	No. of Measurements
Well A							
Zone 1 (Pepper Shale)	36.53	43.48	236.09	10.31	3.54	12.48	21
Zone 2 (top Maness Shale)	50.35	53.40	247.99	22.61	3.87	10.74	10
Zones 3, 4, and 5 (Condensed Section)	72.42	124.02	806.63	45.07	8.06	8.87	9
Zones 6, 7, and 8 (Lower Maness)	29.46	48.92	385.61	1.80	4.00	12.99	12
Totals	47.19	67.46	419.08	19.95	4.87	11.27	13
Well B							
Zone 1 (Pepper Shale)	31.33	42.77	202.76	1.80	3.85	16.12	27
Zone 2 (top Maness Shale)	57.19	71.38	282.27	12.23	4.63	9.32	8
Zones 3, 4, and 5 (Condensed Section)	81.86	103.65	711.10	33.94	6.11	7.76	8
Zones 6, 7, and 8 (Lower Maness)	43.46	50.63	420.30	13.05	9.38	20.21	12
Totals	53.46	67.11	404.11	15.26	5.99	13.35	13.75

Table 5: Average element compositions for chemo zones from whole-rock elemental analysis for wells A and B.

Well Name and Zones	Average TOC (wt. %)	TOC Range (wt. %)	No. of Measurements
Well A			
Zone 1 (Pepper Shale)	2.15	0.52-3.68	22
Zone 2 (top Maness Shale)	3.37	1.68-4.4	19
Zones 3, 4, and 5 (Condensed Section)	3.21	0.53-5.83	17
Zones 6, 7, and 8 (Lower Maness)	2.38	1.14-3.91	22
Totals	2.78		80
Well B			
Zone 1 (Pepper Shale)	1.56	1.08-3.10	26
Zone 2 (top Maness Shale)	3.27	1.02-5.11	11
Zones 3, 4, and 5 (Condensed Section)	4.27	1.19-6.32	12
Zones 6, 7, and 8 (Lower Maness)	2.03	0.98-4.18	12
Totals	2.78		61

Table 6: TOC measurements broken out by chemo zones for wells A and B.

4. CONCLUSIONS

Within the Late Cretaceous Maness and Pepper Shales of Central Texas, 8 chemostratigraphic zones are observed based on bulk changes in major and minor elements. These zones are used to break up a thick section of seemingly monotonous shale in order to be able to determine the zones with the most organic rich source rock and fit these zones into a sequence stratigraphic framework to make a predictable model.

The 8 chemostratigraphic zones are correlatable between 2 wells spaced 6 miles apart; however, there are distinct changes within a particular zone from well to well based on their locations within the basin and corresponding depositional styles. Well A is located updip in a more proximal location to the paleo-shoreline and tends to have higher terrigenous input than what is seen in well B which is downdip in a more distal position.

Zones 6, 7, and 8 located in the lower Maness Shale unconformably overlie the Buda limestone. These zones contain high percentages of clays and low carbonate content. They were deposited during the initial transgression as sea-level rose over the exposed Cretaceous shelf. TOC is moderate averaging 2.2% and does not show a positive correlation between productivity indicators Cu and Ni indicating marine productivity was most likely not the primary source of organic material. Redox-sensitive elements (V, Mo, and U) are highest in zone 8 indicating preservation of organic matter by anoxia while concentrations of these elements drop considerably in zones 6 and 7. In

these zones, organic matter preservation is by something other than anoxia, perhaps preservation by clays or by rapid sediment burial rates.

Zones 3, 4, and 5 contain the most organic-rich source rock facies and represent maximum basin restriction based on high levels of redox-sensitive elements. These zones were deposited as a condensed section which is associated with a maximum flooding surface within the Maness Shale. Carbonate content is high along with productivity indicators Cu and Ni indicating carbonate deposition controlled by a mix of increased productivity which deposited planktonic debris within the basin and diagenetic carbonate cements. TOC is the highest in these zones and averages 3.7 wt. % and reaches as high as 6.32 wt. % in well B. Preservation of the organic material was made possible by low oxygen levels within the basin at this time.

Zone 2 is located in the upper Maness and is the transition between zones 3, 4, and 5 within the condensed section and the overlying zone 1. An increase is seen in clay content with a corresponding decrease in carbonate content. TOC decreases slightly from what was measured in the previous zones and averages 3.3 wt. %. Productivity and redox-sensitive elements are lower in this zone indicating a possible mix of terrestrially derived and marine productivity driven organic material preserved under anoxic to suboxic conditions.

Zone 1 unconformably underlies the Austin Chalk and is mainly composed of the Pepper Shale. Sediments in zone 1 were deposited as part of the prodelta muds and fine-grained clastics from the Woodbine deltas. Very high levels of clay (average of 68%)

and detrital indicator elements confirm sediments are mainly terrestrially sourced. Organic content is low averaging 1.8 wt. % indicating organic material was diluted by the increased clastic deposition. Low redox-sensitive trace element concentrations indicate these sediments were deposited under oxic to suboxic conditions which poorly preserved the organic material.

Mudstone deposition is complex and depends on many varying depositional processes. There is a great deal of variability in these systems that is often not recognized and requires a closer look on a smaller scale. Looking at variations in elements within a thick mudstone section allows for better characterization of source rock facies as well as characterization of reservoir facies, seal capacity, and fracture stimulation potential.

REFERENCES

Adams, R. L., and J.P. Carr, 2010, Regional depositional systems of the Woodbine, Eagle Ford, and Tuscaloosa of the U.S. Gulf Coast: Gulf Coast Association of Geological Societies Transactions, v. 60, p. 3-27.

Ambrose, W. A., T. F. Hentz, F. Bonnaffe, R. G. Louks, L. F. Brown Jr., F. P. Wang, and E. C. Potter, 2009, Sequence-stratigraphic controls on complex reservoir architecture of highstand fluvial-dominated deltaic and lowstand valley-fill deposits in the Upper Cretaceous (Cenomanian) Woodbine Group, East Texas Field: Regional and local perspectives: AAPG Bulletin, v. 93, p. 231-269.

Breyer, J. A., R. Denne, T. Kosanke, J. M. Spaw, J. E. Funk, P. Christmanson, D. A. Bush, and R. Nelson, 2013, Facies, fracture, pressure, and production in the Eagle Ford Shale (Cretaceous) between the Maverick Basin and the San Marcos Arch, Texas, USA: Paper URTeC 1561402 presented at the Unconventional Resource Technology Conference, Denver, Colorado, 12-14 August 2013.

Calvert, S.E., and T.F. Pedersen, 1993, Geochemistry of recent oxic and anoxic marine sediments: Implications for the geological record: Marine Geology, v. 113, p. 67-88.

Charvat, W. A., and R. C. Grayson, 1981, Anoxic sedimentation in the Eagle Ford Group (Upper Cretaceous) of Central Texas: Gulf Coast Association of Geological Societies Transactions, v. 31, p. 256.

Creany, S. and Q. R. Passey, 1993, Recurring patterns of total organic carbon and source rock quality within a sequence stratigraphic framework: AAPG Bulletin, v. 50, p. 3-24.

Dawson, W. C., 2000, Shale microfacies: Eagle Ford Group (Cenomanian-Turonian) north-central Texas outcrops and subsurface equivalents: Gulf Coast Association of Geological Societies Transactions, v. 50, p. 607-622.

Dawson, W.C., and W.R. Almon, 2010, Eagle Ford Shale variability: Sedimentologic influences on source and reservoir character in an unconventional resource unit: Gulf Coast Association of Geological Societies Transactions, v. 60, p. 181-190.

Dean, W. E., and M.A. Arthur, 1998, Cretaceous western interior seaway drilling project: An overview *in* Stratigraphy and paleoenvironments of the Cretaceous western interior seaway, USA: SEPM Concepts in Sedimentology and Paleontology, ISBN 1-56576-044-1, no. 6, p. 1-10.

Edman, J. D., and J. K. Pitman, 2010, Geochemistry of Eagle Ford Group source rocks and oils from First Shot field area, Texas: Gulf Coast Association of Geological Societies Transactions, v. 60, p. 217-234.

Elder, W. P., and J. I. Kirkland, 1994, Cretaceous paleogeography of the southern western interior region *in* Caputo, M. V., J. A. Peterson, and K. J. Franczyk, eds., Mesozoic Systems of the Rocky Mountain Region, USA: Denver, Rocky Mountain Section, Society of Economic Paleontologists and Mineralogists, p. 457-469.

Halbouty, M. T., 1966, Stratigraphic-trap possibilities in upper Jurassic rocks, San Marcos Arch, Texas: AAPG Bulletin, v. 50, p. 3-24.

Hentz, T. F., and S.C. Ruppel, 2010, Regional lithostratigraphy of the Eagle Ford Shale: Maverick Basin to East Texas Basin: Gulf Coast Association of Geological Societies Transactions, v. 60, p. 325-337.

Jarvie, D. M., 1991, Total organic carbon (TOC) analysis: Chapter 11: Geochemical methods and exploration, *in* Source and Migration Processes and Evaluation Techniques: AAPG Special Volumes p. 113-118.

Jarvie, D. M., 2012, Shale resource systems for oil and gas: part 1-shale-gas resource systems, *in* J. A. Breyer, ed., Shale Reservoirs-Giant Resources for the 21st Century: AAPG Memoir 97, p. 69-87.

Katz, B. J., 2005, Controlling factors on source rock development-a review of productivity, preservation, and sedimentation rate, *in* Harris, N., ed., The Deposition of Organic-Carbon-Rich Sediments: Models, Mechanisms, and Consequences: SEPM Special Publication 82 p. 7-16.

Langford, F. F., and M. M. Blanc-Valleron, 1990, Interpreting rock-eval pyrolysis data using graphs of pyrolizable hydrocarbons vs. total organic carbon: AAPG Bulletin, v. 74, p. 799-804.

Liro, L. M., W. C. Dawson, B. J. Katz, and V. D. Robinson, 1994, Sequence stratigraphic elements and geochemical variability within a "condensed section": Eagle Ford group, east-central Texas: Gulf Coast Association of Geological Societies Transactions, v. 44, p. 392-402.

Mancini, E. A., P. Li, D. A. Goddard, V. Ramirez, and S. C. Talukdar, 2008, Mesozoic (Upper Jurassic-Lower Cretaceous) deep gas reservoir play, central and eastern gulf coastal plain: AAPG Bulletin, v. 92, p. 283-308.

Passey, Q. R., K. M. Bohacs, R. E. Klimentidis, W. L. Esch, and S. Sinha, 2010, From oil-prone source rock to gas-producing shale reservoir – Geologic and petrophysical characterization of unconventional shale-gas reservoirs: SPE 31350, 29 p., <http://www.onepetro.org/mslib/servlet/onepetropreview?id=SPE-131350-MS> Accessed 1 July 2014.

Railroad Commission of Texas, 2014, Wells completed and permitted in the Eagle Ford Shale play, <http://www.rrc.state.tx.us/oil-gas/major-oil-gas-formations/eagle-ford-shale/> Accessed July 19, 2014.

Rowe, H., S. Ruppel, S. Rimmer, and R. Louks, 2009, Core-based chemostratigraphy of the Barnett Shale, Permian Basin, Texas: Gulf Coast Association of Geological Societies Transactions, v. 59, p. 675-686.

Sageman, B. B., and M. A. Arthur, 1994, Early Turonian paleogeographic/paleobathymetric map, western interior, U.S. *in* Caputo, M. V., J. A. Peterson, and K. J. Franczyk, eds., Mesozoic Systems of the Rocky Mountain Region, USA: Denver, Rocky Mountain Section, Society of Economic Paleontologists and Mineralogists, p. 457-469.

Tinnin, B., G. Hildred, and N. Martinez, 2013, Expanding the application of chemostratigraphy within the Cretaceous mudrocks: Estimating total organic carbon and paleoredox facies using major, minor, and trace element geochemistry: URTeC Annual Meeting, Control ID Number 1579472.

Tribovillard, N., T.J. Algeo, T. Lyons, and A. Riboulleau, 2006, Trace metals as paleoredox and paleoproductivity proxies: An update: Chemical Geology, v. 232, p. 12-32.

Wescott, W. A., and W. Hood, 1994, Hydrocarbon generation and migration routes in the East Texas Basin: AAPG Bulletin, v. 78, p. 287-307.

Workman, S. J., and G. M. Grammer, 2013, Integrating depositional facies and sequence stratigraphy in characterizing unconventional reservoirs in the Cretaceous (Cenomanian-Turonian) Eagle Ford Shale, South Texas: Gulf Coast Association of Geological Societies Transactions, v. 63, p. 473-508.

Van Wagoner, J. C., R. M. Mitchum, K. M. Campian, and V. D. Rahmanian, 1990, Siliciclastic sequence stratigraphy in well logs, cores, and outcrops: Concepts for high-resolution correlation of time and facies: American Association of Petroleum Geologists Methods in Exploration Series 7, Tulsa, Oklahoma, 55 p.

Zeng, Z., and M.M. Tice, 2014, Promotion and nucleation of carbonate precipitation during microbial iron reduction: Geobiology, v. 12, p. 362-371.